

Testing Supersymmetry with Lepton Flavor Violating

τ and μ decays

Ernesto Arganda* and María J. Herrero†

Departamento de Física Teórica, UAM/IFT, 28049, Madrid, Spain.

Abstract

In this work the following lepton flavor violating τ and μ decays are studied: $\tau^- \rightarrow \mu^- \mu^- \mu^+$, $\tau^- \rightarrow e^- e^- e^+$, $\mu^- \rightarrow e^- e^- e^+$, $\tau^- \rightarrow \mu^- \gamma$, $\tau^- \rightarrow e^- \gamma$ and $\mu^- \rightarrow e^- \gamma$. We work in a supersymmetric scenario consisting of the minimal supersymmetric standard model particle content, extended by the addition of three heavy right handed Majorana neutrinos and their supersymmetric partners, and where the generation of neutrino masses is done via the seesaw mechanism. Within this context, a significant lepton flavor mixing is generated in the slepton sector due to the Yukawa neutrino couplings, which is transmitted from the high to the low energies via the renormalization group equations. This slepton mixing then generates via loops of supersymmetric particles significant contributions to the rates of $l_j \rightarrow 3l_i$ and the correlated $l_j \rightarrow l_i \gamma$ decays. We analyze here in full detail these rates in terms of the relevant input parameters, which are the usual minimal supergravity parameters and the seesaw parameters. For the $l_j \rightarrow 3l_i$ decays, a full one-loop analytical computation of all the contributing supersymmetric loops is presented. This completes and corrects previous computations in the literature. In the numerical analysis compatibility with the most recent experimental upper bounds on all these τ and μ decays, with the neutrino data, and with the present lower bounds on the supersymmetric particle masses are required. Two typical scenarios with degenerate and hierarchical heavy neutrinos are considered. We will show here that the minimal supergravity and seesaw parameters do get important restrictions from these τ and μ decays in the hierarchical neutrino case.

PACS numbers:

*Electronic address: ernesto.arganda@uam.es

†Electronic address: maria.herrero@uam.es

I. INTRODUCTION

The present strong evidence for lepton flavor changing neutrino oscillations in neutrino data [1] implies the existence of non-zero masses for the light neutrinos, and provides the first experimental clue for physics beyond the Standard Model (SM). These oscillations also give an important information on the neutrino mixing angles of the Maki-Nakagawa-Sakata matrix (U_{MNS}) [2]. The experimentally suggested smallness of the three neutrino masses can be explained in a very simple and elegant way by the seesaw mechanism of neutrino mass generation [3]. This mechanism is usually implemented by the introduction of three heavy right-handed (RH) Majorana neutrinos whose masses, m_{M_i} , can be much higher than the SM particle masses. The smallness of the light neutrino masses, m_{ν_i} , appears naturally due to the induced large suppression by the ratio of the two very distant mass scales that are involved in the 3×3 seesaw mass matrices, the Majorana matrix m_M and the Dirac matrix m_D . For instance, in the one generation case, where the seesaw model predicts $m_\nu \sim m_D^2/m_M$, light neutrino masses in the 0.1 - 1 eV range can be generated with m_D being of the order of the electroweak scale, $v = 174$ GeV, and large m_M of the order of 10^{14} GeV. This huge separation between m_M and the electroweak scale has, however, a serious drawback since it leads to the well known hierarchy problem of the SM, where a tree level Higgs boson mass of the order of v is driven by the radiative corrections involving the Majorana neutrinos to very unnatural high values related to the new scale m_M .

The most elegant solution to this hierarchy problem is provided by the introduction of the symmetry relating fermions and bosons, called supersymmetry (SUSY). When the seesaw mechanism for the neutrino mass generation is implemented in a SUSY context, the SUSY scalar partners of the neutrinos, i.e. the sneutrinos, do also contribute to the radiative corrections of the Higgs boson masses and cancel the dangerous contributions from the Majorana neutrinos, solving in this way the hierarchy problem of the simplest non-SUSY version of the seesaw mechanism.

The best evidence of supersymmetry would be obviously the discovery of the SUSY particles in the present or next generation colliders. However, there are alternative ways to test supersymmetry which are indirect and complementary to the direct SUSY particle searches. These refer to the potential measurement of the SUSY particle contributions, via radiative corrections, to rare processes which are being explored at present and whose

rates are predicted to be highly suppressed in the SM. Among these processes, the Lepton Flavor Violating (LFV) τ and μ decays are probably the most interesting ones for various reasons. On one hand, they get vanishing rates in the SM with massless neutrinos and highly suppressed rates in the SM with massive neutrinos. The smallness of these rates in the non-SUSY version of the seesaw mechanism for neutrino mass generation is due to their suppression by inverse powers of the heavy scale m_M . On the other hand, although these decays have not been seen so far in the present experiments, there are very restrictive upper bounds on their possible rates which imply important restrictions on the new physics beyond the SM. These restrictions apply even more severely to the case of softly broken SUSY theories with massive neutrinos and the seesaw mechanism, since these give rise to higher rates [4], being suppressed by inverse powers of the SUSY breaking scale, $m_{SUSY} \leq 1$ TeV, instead of inverse powers of m_M .

We will be devoted here in particular to the LFV τ and μ decays of type $l_j \rightarrow l_i \gamma$ and $l_j \rightarrow 3l_i$ where the present experimental upper bounds are the most restrictive ones [5, 6, 7, 8, 9], specifically,

$$\begin{aligned}
BR(\tau^- \rightarrow \mu^- \mu^- \mu^+) &< 1.9 \times 10^{-7} \\
BR(\tau^- \rightarrow e^- e^- e^+) &< 2.0 \times 10^{-7} \\
BR(\mu^- \rightarrow e^- e^- e^+) &< 1.0 \times 10^{-12} \\
BR(\tau^- \rightarrow \mu^- \gamma) &< 6.8 \times 10^{-8} \\
BR(\tau^- \rightarrow e^- \gamma) &< 1.1 \times 10^{-7} \\
BR(\mu^- \rightarrow e^- \gamma) &< 1.2 \times 10^{-11}
\end{aligned}$$

Our aim in this paper is to analyze the branching ratios that can be generated for all these processes in the context of the SUSY-seesaw scenario with the minimal SUSY content, i.e the Minimal Supersymmetric Standard Model (MSSM), enhanced by the addition of three RH neutrinos and their corresponding SUSY partners. These LFV processes are induced by loops of SUSY particles which transmit the lepton flavor mixing from the slepton mass matrices to the observable charged lepton sector. The intergenerational mixing in the slepton sector, $(M_{\tilde{l}})_{ij}$, $i \neq j$, is induced in turn by the radiative corrections involving the neutrino Yukawa couplings Y_ν or, similarly, by the running of the soft SUSY parameters in the slepton sector, via the Renormalization Group Equations (RGEs), from the high energy scale, $M_X > m_M$, where the heavy Majorana neutrinos are still active, down to the electroweak scale. We will

assume here a Minimal Supergravity scenario (mSUGRA) with universal soft parameters at M_X and the breaking of the electroweak symmetry being generated radiatively. This scenario is also referred to in the literature as the constrained MSSM (CMSSM).

The above LFV processes have previously been studied in the SUSY-seesaw context by several authors [10, 11, 12, 13, 14], under some specific assumptions for both seesaw parameters, m_D (or Y_ν , since they are related by $m_D = Y_\nu v \sin \beta$, with $\tan \beta = v_2/v_1$ being the ratio between the two MSSM Higgs vacuum expectation values) and m_M , and for the mSUGRA parameters, M_0 , $M_{1/2}$, A_0 , $\text{sign}(\mu)$ and $\tan \beta$.

Our present study of these decay channels updates, completes and corrects the previous analyses in several respects. First we include, by the first time to our knowledge, the full set of SUSY one-loop contributions to the $l_j \rightarrow 3l_i$ decays, namely, the photon, the Z boson, and the Higgs bosons penguin diagrams, and the box diagrams. The most complete computation so far of these $l_j \rightarrow 3l_i$ decays was done in [10] where the contributions from the photon and Z boson penguin diagrams and from the box diagrams were included, but they focused on the particular choice of degenerate heavy Majorana neutrinos and they presented numerical results just for $\mu \rightarrow 3e$ decays. We extend this previous study by including in addition the Higgs penguin diagrams mediated by the three neutral MSSM bosons, H_0 , h_0 and A_0 , and correct their results for the Z penguin contributions. We also extend their study in that we present results for the three decays, $\mu \rightarrow 3e$, $\tau \rightarrow 3\mu$ and $\tau \rightarrow 3e$ and consider both possible scenarios, degenerate and hierarchical heavy neutrinos.

The contributions from the Higgs penguin diagrams, in the SUSY-seesaw model, were firstly analyzed in [13]. They worked in the large $\tan \beta$ limit and used the mass insertion approximation to account for the induced effect from the intergenerational slepton mixing in the SUSY contributing loops. There it was concluded that these Higgs-mediated contributions can be very relevant in the large $\tan \beta$ region, because the radiatively induced LFV Higgs- τ - μ couplings grow as $\tan^2 \beta$ (and, in consequence, the $BR(\tau \rightarrow 3\mu)$ as $\tan^6 \beta$), and also because the SUSY one-loop contributions do not decouple in these couplings. These large $\tan \beta$ enhancement and SUSY non-decoupling behaviour were also found in the LFV Higgs boson decays, $H_0, h_0, A_0 \rightarrow l_i \bar{l}_j$ [15, 16]. A more exhaustive study of the $\tau \rightarrow 3\mu$ and other Higgs-mediated LFV τ decays, including an estimate of the Higgs contributions, were done in [17]. However, these previous numerical estimates of the Higgs contributions to LFV τ and μ decays were done in the context of a generic MSSM (see also [18]), where

the Higgs boson mass, or equivalently m_A^0 , is an input parameter and can take small values of the order of 100 GeV which produces larger rates. A more recent study on the LFV Higgs decays has been done in [19] in the SUSY-GUT $SU(5)$ context. We instead work here in the mSUGRA context where all the MSSM particle masses are quantities derived from the mSUGRA parameters. We will see here that this and the requirement of compatibility with the present experimental lower bounds for all the SUSY particle masses [20] do indeed constraint the contribution from the Higgs penguins.

In the present work we also include the predictions for the $l_j \rightarrow l_i \gamma$ channels which, for the context we work with, are interestingly correlated with the $l_j \rightarrow 3l_i$ rates. This correlation has been studied previously in the generic MSSM context in [17] and in a similar mSUGRA context in [14], but in this later the dominant photon penguin approximation was used. We will update this comparative analysis of the $l_j \rightarrow l_i \gamma$ and $l_j \rightarrow 3l_i$ rates, in the mSUGRA context, including the full contributions, and considering the very recent upper bounds for $\tau \rightarrow \mu \gamma$ [7] and $\tau \rightarrow e \gamma$ [8]. In addition, we also require the input seesaw parameters to be compatible with the present neutrino data. For this comparison with the neutrino data we use the parametrization first introduced in [12] for the study of the $\mu \rightarrow e \gamma$ decay.

Our final goal will be to use the SUSY contributions to all the above LFV τ and μ decays as an efficient way to test the mSUGRA and seesaw parameters. With this goal in mind we will analyze here the size of the branching ratios in terms of the mSUGRA and seesaw parameters and will explore in detail the restrictions imposed from the present experimental bounds. We will find that for some plausible choices of the seesaw parameters, being compatible with neutrino data, there are indeed large excluded regions in the mSUGRA parameter space.

The present work is organized as follows. In section II we will review the basic aspects of the MSSM extended with three RH neutrinos, their SUSY partners and the seesaw mechanism for neutrino mass generation. The lepton flavor mixing in the slepton sector and in the mSUGRA context will be explained in section III. There we also include the exact diagonalization of the sfermion mass matrices, both in the slepton and in the sneutrino sectors. The analytical results of the LFV $l_j \rightarrow 3l_i$ decays will be presented in section IV. The numerical results for all the LFV τ and μ decays will be presented in section V. Finally, section VI will be devoted to the conclusions.

II. THE MSSM EXTENDED WITH RH NEUTRINOS AND SNEUTRINOS

In this section we briefly review the additional basic ingredients that are needed to extend the MSSM in order to include three right handed neutrinos, their corresponding SUSY partners, i.e. the sneutrinos, and the generation of neutrino masses by the seesaw mechanism. We follow closely the notation of refs. [12, 16] to describe the SUSY-seesaw scenario and the connection with neutrino data. For the other sectors of the MSSM we assume here the standard conventions as defined, for instance, in [21, 22].

We start with the Yukawa-sector of the MSSM-seesaw that contains the three left handed (LH) SM neutrinos $\nu_{L,i}^o$ and three extra right handed (RH) massive neutrinos $\nu_{R,i}^o$, whose Yukawa interactions provide, after spontaneous electroweak symmetry breaking, together with the right handed neutrino masses, the following mass Lagrangian containing the Dirac and Majorana mass terms,

$$-L_{mass}^\nu = \frac{1}{2}(\overline{\nu_L^o}, (\overline{\nu_R^o})^C)M^\nu \begin{pmatrix} (\nu_L^o)^C \\ \nu_R^o \end{pmatrix} + h.c., \quad (1)$$

where,

$$M^\nu = \begin{pmatrix} 0 & m_D \\ m_D^T & m_M \end{pmatrix}. \quad (2)$$

Here m_D is the 3×3 Dirac mass matrix that is related to the 3×3 Yukawa coupling matrix Y_ν and the MSSM Higgs vacuum expectation value, $\langle H_2 \rangle = v_2 = v \sin \beta$ with $v = 174$ GeV, by $m_D = Y_\nu \langle H_2 \rangle$. The other MSSM Higgs doublet gives masses to the charged leptons by $m_l = Y_l \langle H_1 \rangle$, where Y_l are the Yukawa couplings of the charged leptons and $\langle H_1 \rangle = v_1 = v \cos \beta$. The remaining 3×3 mass matrix involved in the seesaw mechanism, m_M , is real, non singular and symmetric, and provides the masses for the three RH neutrinos

The mass matrix M^ν is a 6×6 complex symmetric matrix that can be diagonalized by a 6×6 unitary matrix U^ν in the following way:

$$U^{\nu T} M^\nu U^\nu = \hat{M}^\nu = \text{diag}(m_{\nu_1}, m_{\nu_2}, m_{\nu_3}, m_{N_1}, m_{N_2}, m_{N_3}). \quad (3)$$

This gives 3 light Majorana neutrino mass eigenstates ν_i , with masses m_{ν_i} (i=1,2,3), and three heavy ones N_i , with masses m_{N_i} (i=1,2,3), which are related to the weak eigenstates

via,

$$\begin{pmatrix} \nu_L^0 \\ (\nu_R^0)^C \end{pmatrix} = U^{\nu*} \begin{pmatrix} \nu_L \\ N_L \end{pmatrix} \quad \text{and} \quad \begin{pmatrix} (\nu_L^0)^C \\ \nu_R^0 \end{pmatrix} = U^\nu \begin{pmatrix} \nu_R \\ N_R \end{pmatrix}. \quad (4)$$

The seesaw mechanism for neutrino mass generation assumes a large separation between the two mass scales involved in m_D and m_M matrices. More specifically, we shall assume here that all matrix elements of m_D are much smaller than those of m_M , $m_D \ll m_M$, and the predictions of the seesaw model are then given in power series of a matrix defined as,

$$\xi \equiv m_D m_M^{-1}. \quad (5)$$

In particular, the previous diagonalization of the mass matrix M^ν can be solved in power series of ξ . For simplicity, we choose to work here and in the rest of this paper, in a flavor basis where the RH Majorana mass matrix, m_M , and the charged lepton mass matrix, m_l , are flavor diagonal. This means that all flavor mixing of the LH sector is included in the mixing matrix U_{MNS} . By working to the lowest orders of these power series expansions one finds, in the flavor basis, the following neutrino 3×3 matrices,

$$\begin{aligned} m_\nu &= -m_D \xi^T + \mathcal{O}(m_D \xi^3) \simeq -m_D m_M^{-1} m_D^T \\ m_N &= m_M + \mathcal{O}(m_D \xi) \simeq m_M. \end{aligned} \quad (6)$$

Here, m_N is already diagonal, but m_ν is not yet diagonal. The rotation from this flavor basis to the mass eigenstate basis is finally given by the MNS unitary matrix, U_{MNS} . Thus,

$$\begin{aligned} m_\nu^{diag} &= U_{MNS}^T m_\nu U_{MNS} = \text{diag}(m_{\nu_1}, m_{\nu_2}, m_{\nu_3}), \\ m_N^{diag} &= m_N = \text{diag}(m_{N_1}, m_{N_2}, m_{N_3}), \end{aligned} \quad (7)$$

and the diagonalization of M^ν in eqs. (2) and (3) can be performed by the following unitary 6×6 matrix:

$$U^\nu = \begin{pmatrix} (1 - \frac{1}{2} \xi^* \xi^T) U_{MNS} & \xi^* (1 - \frac{1}{2} \xi^T \xi^*) \\ -\xi^T (1 - \frac{1}{2} \xi^* \xi^T) U_{MNS} & (1 - \frac{1}{2} \xi^T \xi^*) \end{pmatrix} + \mathcal{O}(\xi^4). \quad (8)$$

As for the U_{MNS} matrix, we use the standard parametrization given by,

$$U_{MNS} = \begin{pmatrix} c_{12}c_{13} & s_{12}c_{13} & s_{13}e^{-i\delta} \\ -s_{12}c_{23} - c_{12}s_{23}s_{13}e^{i\delta} & c_{12}c_{23} - s_{12}s_{23}s_{13}e^{i\delta} & s_{23}c_{13} \\ s_{12}s_{23} - c_{12}c_{23}s_{13}e^{i\delta} & -c_{12}s_{23} - s_{12}c_{23}s_{13}e^{i\delta} & c_{23}c_{13} \end{pmatrix} \text{diag}(1, e^{i\alpha}, e^{i\beta}). \quad (9)$$

where $c_{ij} \equiv \cos \theta_{ij}$ and $s_{ij} \equiv \sin \theta_{ij}$.

Regarding the sneutrino sector, and because of SUSY, the introduction of three RH neutrinos, ν_R , leads to the addition of the three corresponding SUSY partners, $\tilde{\nu}_R$. Thus, there are two complex scalar fields $\tilde{\nu}_L$ and $\tilde{\nu}_R$ per generation, as in the charged slepton case where there are \tilde{l}_L and \tilde{l}_R . The difference is that in the sneutrino sector, the seesaw matrix ξ is involved, as in the neutrino sector, and gives rise to a natural suppression of the RH sneutrino components in the relevant mass eigenstates. This fact makes the diagonalization procedure simpler in the sneutrino sector than in the charged slepton one. In order to understand properly this feature of the MSSM-seesaw model, we will illustrate in the following the simplest case of one generation, where this suppression already manifests. For this, we follow closely [23]. The generalization of this decoupling behaviour of the $\tilde{\nu}_R$ components to the three generations case is straightforward and we omit to show it here, for brevity.

One starts by adding the new terms in the MSSM Lagrangian that involve the ν_R and/or $\tilde{\nu}_R$. In particular, the usual MSSM soft SUSY breaking potential must be modified to include new mass and coupling terms for the right handed sneutrinos, which for the one generation case are the following,

$$V_{soft}^{\tilde{\nu}} = m_{\tilde{M}}^2 \tilde{\nu}_R^* \tilde{\nu}_R - \left(\frac{g}{\sqrt{2}m_W} \epsilon_{ij} \frac{m_D A_\nu}{\sin \beta} H_2^i \tilde{l}_L^j \tilde{\nu}_R^* + h.c. \right) + (m_M B_M \tilde{\nu}_R^* \tilde{\nu}_R + h.c.) \quad (10)$$

where $m_{\tilde{M}}$, A_ν and B_M are the new soft breaking parameters. These are in addition to the usual soft parameters of the slepton sector, $m_{\tilde{L}}$, $m_{\tilde{E}}$ and A_l . The sneutrino mass terms of the MSSM-seesaw model can then be written in the one generation case as,

$$-\mathcal{L}_{mass}^{\nu} = \begin{pmatrix} Re(\tilde{\nu}_L) & Re(\tilde{\nu}_R) & Im(\tilde{\nu}_L) & Im(\tilde{\nu}_R) \end{pmatrix} \begin{pmatrix} M_+^2 & 0 \\ 0 & M_-^2 \end{pmatrix} \begin{pmatrix} Re(\tilde{\nu}_L) \\ Re(\tilde{\nu}_R) \\ Im(\tilde{\nu}_L) \\ Im(\tilde{\nu}_R) \end{pmatrix} \quad (11)$$

with,

$$M_{\pm}^2 = \begin{pmatrix} m_{\tilde{L}}^2 + m_D^2 + \frac{1}{2}m_Z^2 \cos 2\beta & m_D(A_\nu - \mu \cot \beta \pm m_M) \\ m_D(A_\nu - \mu \cot \beta \pm m_M) & m_{\tilde{M}}^2 + m_D^2 + m_M^2 \pm 2B_M m_M \end{pmatrix} \quad (12)$$

Notice that, in the sneutrino sector, there are several mass scales involved, the soft SUSY-breaking parameters, $m_{\tilde{L}}$, $m_{\tilde{M}}$, B_M and A_ν , the Dirac mass m_D , the μ -mass parameter, the Z boson mass m_Z and the Majorana neutrino mass m_M . Our basic assumption in all this work is that m_M is much heavier than the other mass scales involved (except M_X), $m_M \gg m_D, m_Z, \mu, m_{\tilde{L}}, m_{\tilde{M}}, A_\nu, B_M$. The size of B_M has been discussed in the literature [23] and seems more controversial. For simplicity, we shall assume here that this is also smaller than m_M . In this large m_M limit, the diagonalization of the previous sneutrino squared mass matrix is simpler and leads to four mass eigenstates, two of which are light, ξ_1^l, ξ_2^l and two heavy, ξ_1^h, ξ_2^h . In the leading orders of the series expansion in powers of ξ the mass eigenstates and their corresponding mass eigenvalues are given by (We correct in the definitions of M_{\pm}^2 and ξ_2^l some typos with wrong signs of ref. [16]),

$$\begin{aligned} \xi_1^l &= \sqrt{2}(Re(\tilde{\nu}_L) - \xi Re(\tilde{\nu}_R)) ; \xi_2^l = \sqrt{2}(Im(\tilde{\nu}_L) + \xi Im(\tilde{\nu}_R)) \\ \xi_1^h &= \sqrt{2}(Re(\tilde{\nu}_R) + \xi Re(\tilde{\nu}_L)) ; \xi_2^h = \sqrt{2}(Im(\tilde{\nu}_R) - \xi Im(\tilde{\nu}_L)) \\ m_{\xi_{1,2}^l}^2 &= m_{\tilde{L}}^2 + \frac{1}{2}m_Z^2 \cos 2\beta \mp 2m_D(A_\nu - \mu \cot \beta - B_M)\xi \\ m_{\xi_{1,2}^h}^2 &= m_M^2 \pm 2B_M m_M + m_{\tilde{M}}^2 + 2m_D^2 \end{aligned} \quad (13)$$

Here we can see that the heavy states $\xi_{1,2}^h$ will couple very weakly to the rest of particles of the MSSM via their $\tilde{\nu}_L$ component, which is highly suppressed by the small factor ξ and, therefore, it is a good approximation to ignore them and keep just the light states $\xi_{1,2}^l$, which are made mainly of $\tilde{\nu}_L$ and its complex conjugate $\tilde{\nu}_L^*$. One says then that the heavy sneutrinos decouple from the low energy physics.

The generalization of the previous argument to the three generations case leads to the conclusion that, in the seesaw limit, $\xi \ll 1$, the physical sneutrino eigenstates, $\tilde{\nu}_\beta$ ($\beta = 1, 2, 3$) are made mainly of the $\tilde{\nu}_{L,l}$ states with $l = e, \mu, \tau$ respectively, and their corresponding complex conjugates. The process from the weak eigenstates to the mass eigenstates is simplified to the diagonalization of a 3×3 sneutrino mass matrix. This is to be compared with the more complex case of charged sleptons where the corresponding process requires the diagonalization of a 6×6 slepton mass matrix. This will be presented in the next section, where the most general case with lepton flavor mixing is considered.

To end this section, we shortly comment on the parameterization that we use to make contact with the neutrino data. It was first introduced in [12] to study the $\mu \rightarrow e\gamma$ decay and used later by many other authors. The advantage of this parameterization is that instead of using as input parameters the seesaw mass matrices m_D and m_M it uses the three physical light neutrino masses, m_{ν_i} , the three physical heavy neutrino masses, m_{N_i} , the U_{MNS} matrix, and a general complex 3×3 orthogonal matrix R . With our signs and matrix conventions, the relation between the seesaw mass matrices and these other more physical quantities is given by,

$$m_D^T = i m_N^{diag\,1/2} R m_\nu^{diag\,1/2} U_{MNS}^+ \quad (14)$$

where $R^T R = 1$ and, as we have said, $m_{N_i} \simeq m_{M_i}$. Thus, instead of proposing directly possible textures for m_D , or Y_ν , one proposes possible values for $m_{N_1}, m_{N_2}, m_{N_3}$ and R , and sets $m_{\nu_1}, m_{\nu_2}, m_{\nu_3}$ and U_{MNS} to their suggested values from the experimental data. Notice that any hypothesis for R different from the unit matrix will lead to an additional lepton flavor mixing, besides the one introduced by the U_{MNS} . Notice also that the previous relation holds at the energy scale m_M , and to use it properly one must apply the Renormalization Group Equations to run the input experimental data m_ν^{diag} and U_{MNS} from the low energies m_W up to m_M . Therefore, we will also include these running effects in the numerical results for all the branching ratios presented in this work.

Regarding the matrix R , we will consider the following parameterization:

$$R = \begin{pmatrix} c_2 c_3 & -c_1 s_3 - s_1 s_2 c_3 & s_1 s_3 - c_1 s_2 c_3 \\ c_2 s_3 & c_1 c_3 - s_1 s_2 s_3 & -s_1 c_3 - c_1 s_2 s_3 \\ s_2 & s_1 c_2 & c_1 c_2 \end{pmatrix}. \quad (15)$$

where $c_i \equiv \cos \theta_i$, $s_i \equiv \sin \theta_i$ and θ_1, θ_2 and θ_3 are arbitrary complex angles. This parameterization was proposed in ref. [12] for the study of $\mu \rightarrow e\gamma$ decays. It has also been considered in ref. [24, 25] with specific values for the θ_i angles to study the implications for baryogenesis in the case of hierarchical neutrinos. And it has also been considered by [16] to study the LFV Higgs boson decays into $l_i \bar{l}_j$.

Finally, for the numerical estimates in this work, we will consider the following two plausible scenarios, at the low energies, being compatible with data:

- Scenario A: with quasi-degenerate light and degenerate heavy neutrinos,

$$\begin{aligned}
m_{\nu_1} &= 0.2 \text{ eV}, m_{\nu_2} = m_{\nu_1} + \frac{\Delta m_{sol}^2}{2m_{\nu_1}}, m_{\nu_3} = m_{\nu_1} + \frac{\Delta m_{atm}^2}{2m_{\nu_1}}, \\
m_{N_1} &= m_{N_2} = m_{N_3} = m_N
\end{aligned}
\tag{16}$$

- Scenario B: with hierarchical light and hierarchical heavy neutrinos,

$$\begin{aligned}
m_{\nu_1} &\simeq 0 \text{ eV}, m_{\nu_2} = \sqrt{\Delta m_{sol}^2}, m_{\nu_3} = \sqrt{\Delta m_{atm}^2}, \\
m_{N_1} &\leq m_{N_2} < m_{N_3}
\end{aligned}
\tag{17}$$

In the two above scenarios, we will fix the input low energy data to the following values, $\sqrt{\Delta m_{sol}^2} = 0.008 \text{ eV}$, $\sqrt{\Delta m_{atm}^2} = 0.05 \text{ eV}$, $\theta_{12} = \theta_{sol} = 30^\circ$, $\theta_{23} = \theta_{atm} = 45^\circ$, $\theta_{13} = 0^\circ$ and $\delta = \alpha = \beta = 0$ (See for instance, ref. [26]). Some results will also be presented for the alternative choice of small but non-vanishing θ_{13} .

III. GENERATION OF FLAVOR MIXING IN THE SLEPTON SECTOR

Once the three ν_R and the three $\tilde{\nu}_R$ are added to the MSSM particle content, lepton flavor mixing is generated in the slepton sector. This can be seen as the result of a misalignment between the rotations leading to the mass eigenstate basis of sleptons with respect to the one of leptons, which is generically present in the SUSY-seesaw models. This misalignment is radiatively generated from the Yukawa couplings of the Majorana neutrinos and can be sizable, in both, the charged slepton and sneutrino sectors. Usually, it is implemented via the Renormalization Group Equations (RGEs), which we take within the context of mSUGRA extended with three right-handed neutrinos and their SUSY partners. In consequence, we assume here universal soft-SUSY-breaking parameters at the large energies $M_X \gg m_M$, which must now include the corresponding parameters of the neutrino and sneutrino sectors, namely,

$$\begin{aligned}
(m_{\tilde{L}})_{ij}^2 &= M_0^2 \delta_{ij}, (m_{\tilde{E}})_{ij}^2 = M_0^2 \delta_{ij}, (m_{\tilde{M}})_{ij}^2 = M_0^2 \delta_{ij} \\
(A_l)_{ij} &= A_0 (Y_l)_{ij}, (A_\nu)_{ij} = A_0 (Y_\nu)_{ij}, i, j = 1, 2, 3
\end{aligned}
\tag{18}$$

Here, M_0 and A_0 are the usual universal soft SUSY breaking parameters in mSUGRA, $(Y_l)_{ij} = Y_{l_i} \delta_{ij}$ with $Y_{l_i} = m_{l_i}/v_1$, and $(Y_\nu)_{ij} = (m_D)_{ij}/v_2$. Notice that we have used the 3×3 matrix form with $i, j = 1, 2, 3$ or equivalently $i, j = e, \mu, \tau$.

The effects of the running from M_X down to m_M on the soft mass matrices of the slepton sector are found then by solving the RGEs which now include the corresponding terms and equations for the Yukawas of the neutrinos and soft breaking parameters of the sneutrino sector, as they are active particles in this energy range. Below the energy scales m_M , the right handed neutrinos decouple and the effects of running from m_M down to the electroweak scale on the various parameters are obtained by solving the RGEs but now without the terms and equations containing the Yukawas and soft breaking neutrino parameters. The obtained values at the electroweak scale of the various SUSY parameters are the relevant ones in order to build the slepton and sneutrino mass matrices that will be presented below.

To solve numerically the RGEs we use the Fortran code SPheno [27] that we have adapted to include the full flavor structure of the 3×3 soft SUSY breaking mass and trilinear coupling matrices and of the Yukawa coupling matrices. This program solves the full RGEs (i.e. including the commented extra equations and neutrino terms) in the two loops approximation, computes the MSSM spectra at low energies, and uses as inputs the universal mSUGRA parameters, M_0 , A_0 , $M_{1/2}$; the value of $\tan\beta$ at the electroweak scale, and the sign of the μ mass parameter. The value of M_X is derived from the unification condition for the $SU(2)$ and $U(1)$ couplings, $g_1 = g_2$. For all the numerical analysis performed in this work, we have got very close values to $M_X = 2 \times 10^{16}$ GeV. The value of $|\mu|$ is derived from the requirement of the proper radiative electroweak symmetry breaking.

We present next the slepton mass matrices, relevant to low energies, that include the lepton mixing generated from the neutrino Yukawa couplings by the RGEs. For the charged slepton case and referred to the $(\tilde{e}_L, \tilde{e}_R, \tilde{\mu}_L, \tilde{\mu}_R, \tilde{\tau}_L, \tilde{\tau}_R)$ basis, the squared mass matrix can be written as follows,

$$M_{\tilde{l}}^2 = \begin{pmatrix} M_{LL}^{ee2} & M_{LR}^{ee2} & M_{LL}^{e\mu2} & M_{LR}^{e\mu2} & M_{LL}^{e\tau2} & M_{LR}^{e\tau2} \\ M_{RL}^{ee2} & M_{RR}^{ee2} & M_{RL}^{e\mu2} & M_{RR}^{e\mu2} & M_{RL}^{e\tau2} & M_{RR}^{e\tau2} \\ M_{LL}^{\mu e2} & M_{LR}^{\mu e2} & M_{LL}^{\mu\mu2} & M_{LR}^{\mu\mu2} & M_{LL}^{\mu\tau2} & M_{LR}^{\mu\tau2} \\ M_{RL}^{\mu e2} & M_{RR}^{\mu e2} & M_{RL}^{\mu\mu2} & M_{RR}^{\mu\mu2} & M_{RL}^{\mu\tau2} & M_{RR}^{\mu\tau2} \\ M_{LL}^{\tau e2} & M_{LR}^{\tau e2} & M_{LL}^{\tau\mu2} & M_{LR}^{\tau\mu2} & M_{LL}^{\tau\tau2} & M_{LR}^{\tau\tau2} \\ M_{RL}^{\tau e2} & M_{RR}^{\tau e2} & M_{RL}^{\tau\mu2} & M_{RR}^{\tau\mu2} & M_{RL}^{\tau\tau2} & M_{RR}^{\tau\tau2} \end{pmatrix} \quad (19)$$

where,

$$\begin{aligned}
M_{LL}^{ij2} &= m_{\tilde{L},ij}^2 + v_1^2 (Y_l^\dagger Y_l)_{ij} + m_Z^2 \cos 2\beta \left(-\frac{1}{2} + \sin^2 \theta_W \right) \delta_{ij} \\
M_{RR}^{ij2} &= m_{\tilde{E},ij}^2 + v_1^2 (Y_l^\dagger Y_l)_{ij} - m_Z^2 \cos 2\beta \sin^2 \theta_W \delta_{ij} \\
M_{LR}^{ij2} &= v_1 (A_l^{ij})^* - \mu Y_l^{ij} v_2 \\
M_{RL}^{ij2} &= (M_{LR}^{ij2})^*
\end{aligned} \tag{20}$$

The soft SUSY breaking mass matrices and trilinear coupling matrices above, $m_{\tilde{L},ij}$, $m_{\tilde{E},ij}$ and A_l^{ij} , with $i, j = e, \mu, \tau$, refer to their corresponding values at the electroweak scale which we get with the SPheno program.

After numerical diagonalization of the $M_{\tilde{l}}^2$ matrix one gets the physical slepton masses and the six mass eigenstates $(\tilde{l}_1, \dots, \tilde{l}_6) \equiv \tilde{l}$ which are related to the previous weak eigenstates $(\tilde{e}_L, \dots, \tilde{\tau}_R) \equiv \tilde{l}'$ by $\tilde{l}' = R^{(l)} \tilde{l}$, where $R^{(l)}$ is a 6×6 rotation matrix such that,

$$M_{\tilde{l}'diag}^2 = R^{(l)} M_{\tilde{l}}^2 R^{(l)\dagger} = \text{diag}(m_{\tilde{l}_1}^2, \dots, m_{\tilde{l}_6}^2). \tag{21}$$

For the sneutrino sector, the 3×3 squared mass matrix, referred to the $\tilde{\nu}' = (\tilde{\nu}_{e,L}, \tilde{\nu}_{\mu,L}, \tilde{\nu}_{\tau,L})$ basis can be written as follows,

$$M_{\tilde{\nu}}^2 = \begin{pmatrix} m_{\tilde{L},ee}^2 + \frac{1}{2}m_Z^2 \cos 2\beta & m_{\tilde{L},e\mu}^2 & m_{\tilde{L},e\tau}^2 \\ m_{\tilde{L},\mu e}^2 & m_{\tilde{L},\mu\mu}^2 + \frac{1}{2}m_Z^2 \cos 2\beta & m_{\tilde{L},\mu\tau}^2 \\ m_{\tilde{L},\tau e}^2 & m_{\tilde{L},\tau\mu}^2 & m_{\tilde{L},\tau\tau}^2 + \frac{1}{2}m_Z^2 \cos 2\beta \end{pmatrix} \tag{22}$$

where $m_{\tilde{L},ij}^2$ are the same as in the previous charged slepton squared mass matrix. After diagonalization of the $M_{\tilde{\nu}}^2$ matrix one gets the relevant physical sneutrino masses and eigenstates, $\tilde{\nu}_\beta$ ($\beta = 1, 2, 3$) which are related to the previous states $\tilde{\nu}'_\alpha$ by the corresponding 3×3 rotation matrix, $\tilde{\nu}' = R^{(\nu)} \tilde{\nu}$, and is such that,

$$M_{\tilde{\nu}'diag}^2 = R^{(\nu)} M_{\tilde{\nu}}^2 R^{(\nu)\dagger} = \text{diag}(m_{\tilde{\nu}_1}^2, m_{\tilde{\nu}_2}^2, m_{\tilde{\nu}_3}^2). \tag{23}$$

Finally, in order to illustrate later the size of the misalignment effects in the slepton sector we define the following dimensionless parameters,

$$\delta_{LL}^{ij} = \frac{M_{LL}^{ij2}}{\tilde{m}^2} \tag{24}$$

$$\delta_{LR}^{ij} = \frac{M_{LR}^{ij2}}{\tilde{m}^2} \tag{25}$$

$$\delta_{RR}^{ij} = \frac{M_{RR}^{ij2}}{\tilde{m}^2} \tag{26}$$

where

$$\tilde{m}^2 = \left(m_{\tilde{l}_1}^2 m_{\tilde{l}_2}^2 m_{\tilde{l}_3}^2 m_{\tilde{l}_4}^2 m_{\tilde{l}_5}^2 m_{\tilde{l}_6}^2 \right)^{1/6} \quad (27)$$

is an average slepton squared mass. These parameters have also been considered by other authors in a more model independent approach and with the purpose of getting bounds from experimental data. Some of these bounds can be found in [28, 29, 30].

For all the numerical results presented in this paper, we will set values for all the following input parameters and physical quantities:

- mSUGRA parameters: $M_0, M_{1/2}, A_0, \text{sign}(\mu)$ and $\tan\beta$.
- seesaw parameters: $m_{N_1}, m_{N_2}, m_{N_3}$ and R (or equivalently $\theta_1, \theta_2, \theta_3$).
- physical quantities: $m_{\nu_1}, m_{\nu_2}, m_{\nu_3}, U_{MNS}$

IV. ANALYTICAL RESULTS FOR THE $l_j^- \rightarrow l_i^- l_i^- l_i^+$ DECAYS

In this section we present the analytical results for the LFV τ and μ decays into three leptons with the same flavor, within the mSUGRA-seesaw context that we have presented in the previous sections. We perform a complete one-loop computation of the τ and μ decay widths for all the three possible channels, $\tau^- \rightarrow \mu^- \mu^- \mu^+$, $\tau^- \rightarrow e^- e^- e^+$ and $\mu^- \rightarrow e^- e^- e^+$, and include all the contributing SUSY loops. We present each contribution separately, γ -penguin, Z -penguin, Higgs-penguin and boxes. The contributions from the Higgs-penguin diagrams are, to our knowledge, computed exactly by the first time here. We have also reviewed the analytical results in [10] and correct their results for the Z -penguin contributions. Notice that we make the computation in the physical mass eigenstate basis. That is, we consider the one-loop contributions from charged sleptons, \tilde{l}_X ($X = 1, \dots, 6$), sneutrinos $\tilde{\nu}_X$ ($X = 1, 2, 3$), charginos $\tilde{\chi}_A^-$ ($A = 1, 2$), and neutralinos $\tilde{\chi}_A^0$ ($A = 1, \dots, 4$). In all this section we follow closely the notation and way of presentation of [10]. The interactions in the physical mass eigenstate basis that are needed for this computation are collected in the form of Feynman rules in Appendix A.

First, we define the amplitudes for the $l_j^-(p) \rightarrow l_i^-(p_1) l_i^-(p_2) l_i^+(p_3)$ decays as the sum of the various contributions,

$$T(l_j^- \rightarrow l_i^- l_i^- l_i^+) = T_{\gamma\text{-penguin}} + T_{Z\text{-penguin}} + T_{H\text{-penguin}} + T_{\text{boxes}}. \quad (28)$$

In the following we present the results for these contributions in terms of some convenient form factors.

A. The γ -penguin contributions

The diagrams where a photon is exchanged are called γ -penguin diagrams and are shown in fig. 1. The result for the γ -penguin amplitude contributing to the $l_j^- \rightarrow l_i^- l_i^- l_i^+$ decays is usually written as,

$$T_{\gamma\text{-penguin}} = \bar{u}_i(p_1) \left[q^2 \gamma_\mu (A_1^L P_L + A_1^R P_R) + i m_{l_j} \sigma_{\mu\nu} q^\nu (A_2^L P_L + A_2^R P_R) \right] u_j(p) \times \frac{e^2}{q^2} \bar{u}_i(p_2) \gamma^\mu v_i(p_3) - (p_1 \leftrightarrow p_2) \quad (29)$$

where q is the photon momentum and e is the electric charge. The photon-penguin amplitude has two contributions in the MSSM-seesaw from the chargino and neutralino sectors respectively, as can be seen in the structure of the form factors,

$$A_a^{L,R} = A_a^{(n)L,R} + A_a^{(c)L,R}, \quad a = 1, 2 \quad (30)$$

The neutralino contributions are given by

$$A_1^{(n)L} = \frac{1}{576\pi^2} N_{iAX}^R N_{jAX}^{R*} \frac{1}{m_{\tilde{l}_X}^2} \frac{2 - 9x_{AX} + 18x_{AX}^2 - 11x_A^3 + 6x_{AX}^3 \log x_{AX}}{(1 - x_{AX})^4} \quad (31)$$

$$A_2^{(n)L} = \frac{1}{32\pi^2} \frac{1}{m_{\tilde{l}_X}^2} \left[N_{iAX}^L N_{jAX}^{L*} \frac{1 - 6x_{AX} + 3x_{AX}^2 + 2x_{AX}^3 - 6x_{AX}^2 \log x_{AX}}{6(1 - x_{AX})^4} + N_{iAX}^R N_{jAX}^{R*} \frac{m_{l_i}}{m_{l_j}} \frac{1 - 6x_{AX} + 3x_{AX}^2 + 2x_{AX}^3 - 6x_{AX}^2 \log x_{AX}}{6(1 - x_{AX})^4} + N_{iAX}^L N_{jAX}^{R*} \frac{m_{\tilde{\chi}_A^0}}{m_{l_j}} \frac{1 - x_{AX}^2 + 2x_{AX} \log x_{AX}}{(1 - x_{AX})^3} \right] \quad (32)$$

$$A_a^{(n)R} = A_a^{(n)L} \Big|_{L \leftrightarrow R} \quad (33)$$

where $x_{AX} = m_{\tilde{\chi}_A^0}^2 / m_{\tilde{l}_X}^2$. On the other hand, the chargino contributions are

$$A_1^{(c)L} = -\frac{1}{576\pi^2} C_{iAX}^R C_{jAX}^{R*} \frac{1}{m_{\tilde{\nu}_X}^2} \frac{16 - 45x_{AX} + 36x_{AX}^2 - 7x_A^3 + 6(2 - 3x_{AX}) \log x_{AX}}{(1 - x_{AX})^4} \quad (34)$$

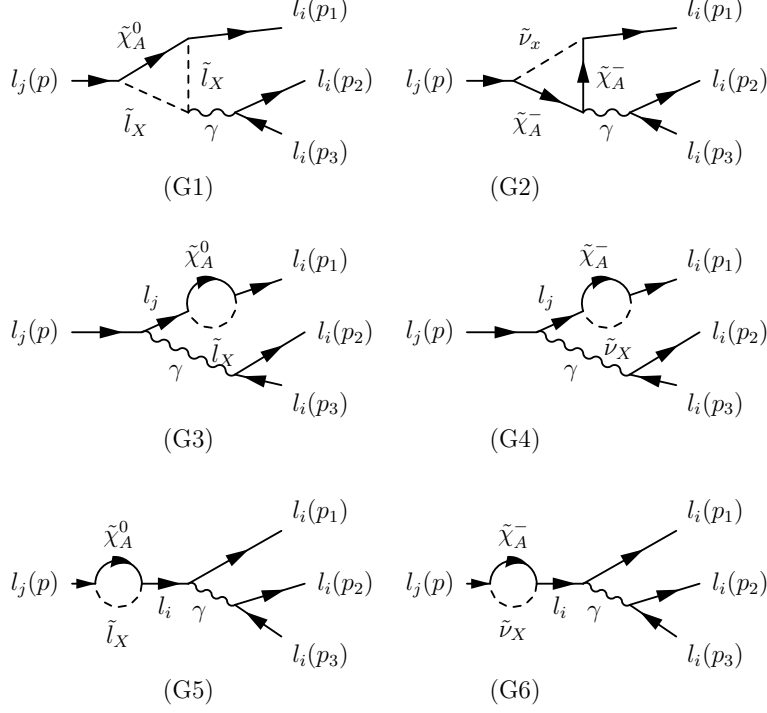


FIG. 1: γ -penguin diagrams contributing to the $l_j^- \rightarrow l_i^- l_i^- l_i^+$ decay

$$\begin{aligned}
A_2^{(c)L} &= -\frac{1}{32\pi^2} \frac{1}{m_{\tilde{\nu}_X}^2} \left[C_{iAX}^L C_{jAX}^{L*} \frac{2 + 3x_{AX} - 6x_{AX}^2 + x_{AX}^3 + 6x_{AX} \log x_{AX}}{6(1-x_{AX})^4} \right. \\
&+ C_{iAX}^R C_{jAX}^{R*} \frac{m_{l_i}}{m_{l_j}} \frac{2 + 3x_{AX} - 6x_{AX}^2 + x_{AX}^3 + 6x_{AX} \log x_{AX}}{6(1-x_{AX})^4} \\
&\left. + C_{iAX}^L C_{jAX}^{R*} \frac{m_{\tilde{\chi}_A^-}}{m_{l_j}} \frac{-3 + 4x_{AX} - x_{AX}^2 - 2 \log x_{AX}}{(1-x_{AX})^3} \right] \quad (35)
\end{aligned}$$

$$A_a^{(c)R} = A_a^{(c)L} \Big|_{L \leftrightarrow R} \quad (36)$$

where $x_{AX} = m_{\tilde{\chi}_A^-}^2 / m_{\tilde{\nu}_X}^2$. Notice that in both neutralino and chargino contributions a summation over the indices A and X is understood. Notice also that we have not neglected any of the fermion masses. If we neglect these masses in the previous formulas we get the same result as in [10]. The expressions for the N and C couplings are given in the Appendix A.

B. The Z -penguin contributions

The diagrams where a Z boson is exchanged are called the Z -penguin diagrams and are shown in fig. 2. The amplitude in this case is

$$T_{Z\text{-penguin}} = \frac{1}{m_Z^2} \bar{u}_i(p_1) [\gamma_\mu (F_L P_L + F_R P_R)] u_j(p) \times \bar{u}_i(p_2) \left[\gamma^\mu \left(Z_L^{(l)} P_L + Z_R^{(l)} P_R \right) \right] v_i(p_3) - (p_1 \leftrightarrow p_2) \quad (37)$$

where, as before, $F_{L(R)} = F_{L(R)}^{(n)} + F_{L(R)}^{(c)}$. The expressions for these form factors are the following:

$$F_L^{(n)} = -\frac{1}{16\pi^2} \left\{ N_{iBX}^R N_{jAX}^{R*} \left[2E_{BA}^{R(n)} C_{24}(m_{\tilde{l}_X}^2, m_{\tilde{\chi}_A^0}^2, m_{\tilde{\chi}_B^0}^2) - E_{BA}^{L(n)} m_{\tilde{\chi}_A^0} m_{\tilde{\chi}_B^0} C_0(m_{\tilde{l}_X}^2, m_{\tilde{\chi}_A^0}^2, m_{\tilde{\chi}_B^0}^2) \right] + N_{iAX}^R N_{jAY}^{R*} \left[2Q_{XY}^{\tilde{l}} C_{24}(m_{\tilde{\chi}_A^0}^2, m_{\tilde{l}_X}^2, m_{\tilde{l}_Y}^2) \right] + N_{iAX}^R N_{jAX}^{R*} \left[Z_L^{(l)} B_1(m_{\tilde{\chi}_A^0}^2, m_{\tilde{l}_X}^2) \right] \right\} \quad (38)$$

$$F_R^{(n)} = F_L^{(n)} \Big|_{L \leftrightarrow R} \quad (39)$$

$$F_L^{(c)} = -\frac{1}{16\pi^2} \left\{ C_{iBX}^R C_{jAX}^{R*} \left[2E_{BA}^{R(c)} C_{24}(m_{\tilde{\nu}_X}^2, m_{\tilde{\chi}_A^-}^2, m_{\tilde{\chi}_B^-}^2) - E_{BA}^{L(c)} m_{\tilde{\chi}_A^-} m_{\tilde{\chi}_B^-} C_0(m_{\tilde{\nu}_X}^2, m_{\tilde{\chi}_A^-}^2, m_{\tilde{\chi}_B^-}^2) \right] + C_{iAX}^R C_{jAY}^{R*} \left[2Q_{XY}^{\tilde{\nu}} C_{24}(m_{\tilde{\chi}_A^-}^2, m_{\tilde{\nu}_X}^2, m_{\tilde{\nu}_Y}^2) \right] + C_{iAX}^R C_{jAX}^{R*} \left[Z_L^{(l)} B_1(m_{\tilde{\chi}_A^-}^2, m_{\tilde{\nu}_X}^2) \right] \right\} \quad (40)$$

$$F_R^{(c)} = F_L^{(c)} \Big|_{L \leftrightarrow R} \quad (41)$$

Notice that all the loop functions are evaluated at zero external momenta which is a very good approximation in these decays. That is,

$$B(m_1^2, m_2^2) = B(0, m_1^2, m_2^2) \quad (42)$$

$$C(m_1^2, m_2^2, m_3^2) = C(0, 0, m_1^2, m_2^2, m_3^2) \quad (43)$$

The expressions for the couplings are collected in Appendix A and the loop functions [31] are given in the Appendix B. Notice that our result for the Z -penguin contributions differs significantly from the result in [10]. In fact, these authors did not consider all the diagrams in these Z -penguin contributions, which we think is not justified.

C. The box contributions

The box-type diagrams are shown in fig. 3. We have computed these diagrams and found a result in agreement with [10]. The amplitude for these box contributions can be written

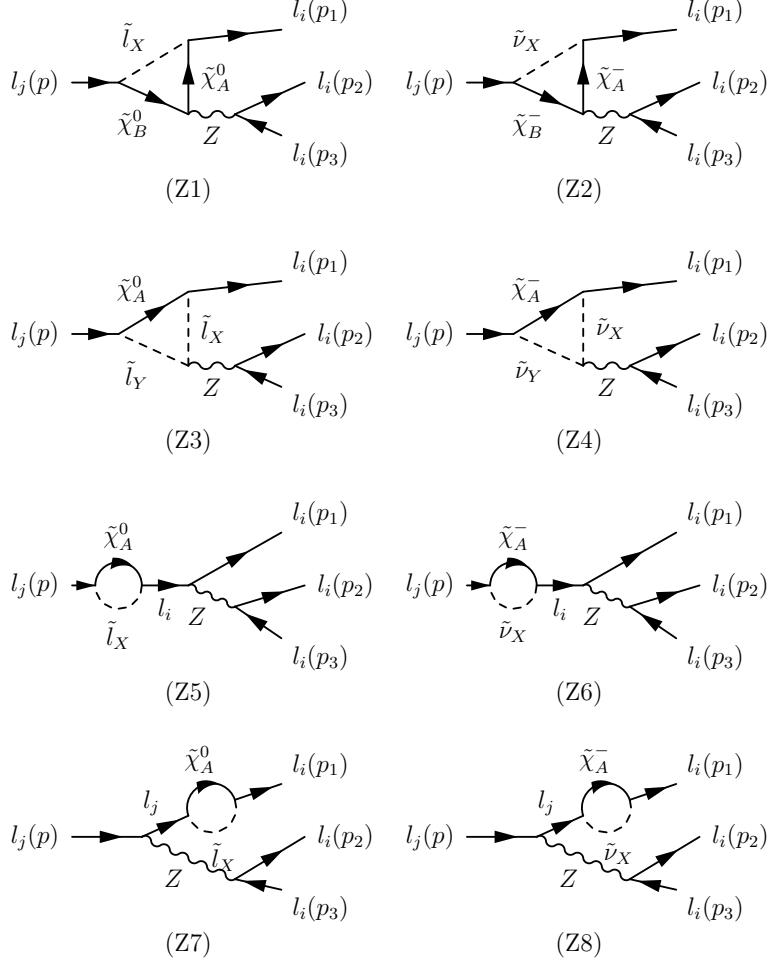


FIG. 2: Z -penguin diagrams contributing to the $l_j^- \rightarrow l_i^- l_i^- l_i^+$ decay

as,

$$\begin{aligned}
T_{\text{boxes}} = & e^2 B_1^L [\bar{u}_i(p_1) (\gamma^\mu P_L) u_j(p)] [\bar{u}_i(p_2) (\gamma_\mu P_L) v_i(p_3)] \\
& + e^2 B_1^R [\bar{u}_i(p_1) (\gamma^\mu P_R) u_j(p)] [\bar{u}_i(p_2) (\gamma_\mu P_R) v_i(p_3)] \\
& + e^2 B_2^L \{ [\bar{u}_i(p_1) (\gamma^\mu P_L) u_j(p)] [\bar{u}_i(p_2) (\gamma_\mu P_R) v_i(p_3)] - (p_1 \leftrightarrow p_2) \} \\
& + e^2 B_2^R \{ [\bar{u}_i(p_1) (\gamma^\mu P_R) u_j(p)] [\bar{u}_i(p_2) (\gamma_\mu P_L) v_i(p_3)] - (p_1 \leftrightarrow p_2) \} \\
& + e^2 B_3^L \{ [\bar{u}_i(p_1) P_L u_j(p)] [\bar{u}_i(p_2) P_L v_i(p_3)] - (p_1 \leftrightarrow p_2) \} \\
& + e^2 B_3^R \{ [\bar{u}_i(p_1) P_R u_j(p)] [\bar{u}_i(p_2) P_R v_i(p_3)] - (p_1 \leftrightarrow p_2) \} \\
& + e^2 B_4^L \{ [\bar{u}_i(p_1) (\sigma_{\mu\nu} P_L) u_j(p)] [\bar{u}_i(p_2) (\sigma^{\mu\nu} P_L) v_i(p_3)] - (p_1 \leftrightarrow p_2) \} \\
& + e^2 B_4^R \{ [\bar{u}_i(p_1) (\sigma_{\mu\nu} P_R) u_j(p)] [\bar{u}_i(p_2) (\sigma^{\mu\nu} P_R) v_i(p_3)] - (p_1 \leftrightarrow p_2) \}
\end{aligned}$$

(44)

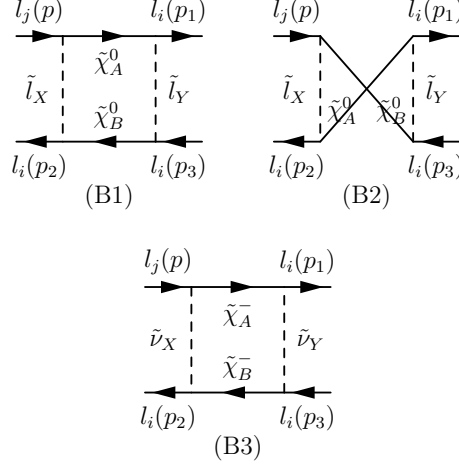


FIG. 3: Box-type diagrams contributing to the $l_j^- \rightarrow l_i^- l_i^- l_i^+$ decay

where

$$B_a^{L,R} = B_a^{(n)L,R} + B_a^{(c)L,R} \quad a = 1, \dots, 4 \quad (45)$$

The different neutralino contributions are,

$$e^2 B_1^{(n)L} = \frac{1}{16\pi^2} \left[\frac{\tilde{D}_0}{2} N_{iAY}^R N_{jAX}^{R*} N_{iBX}^R N_{iBY}^{R*} + D_0 m_{\tilde{\chi}_A^0} m_{\tilde{\chi}_B^0} N_{iBY}^R N_{iBX}^R N_{jAX}^{R*} N_{iAY}^{R*} \right] \quad (46)$$

$$e^2 B_2^{(n)L} = \frac{1}{16\pi^2} \left[\frac{\tilde{D}_0}{4} N_{iAY}^R N_{jAX}^{R*} N_{iBX}^L N_{iBY}^{L*} - \frac{D_0}{2} m_{\tilde{\chi}_A^0} m_{\tilde{\chi}_B^0} N_{iAY}^L N_{jAX}^{R*} N_{iBX}^R N_{iBY}^{L*} \right. \\ \left. - \frac{\tilde{D}_0}{4} N_{iBY}^L N_{iBX}^R N_{jAX}^{R*} N_{iAY}^{L*} + \frac{\tilde{D}_0}{4} N_{iBY}^R N_{iBX}^L N_{jAX}^{R*} N_{iAY}^{L*} \right] \quad (47)$$

$$e^2 B_3^{(n)L} = \frac{1}{16\pi^2} \left[D_0 m_{\tilde{\chi}_A^0} m_{\tilde{\chi}_B^0} N_{iAY}^L N_{jAX}^{R*} N_{iBX}^L N_{iBY}^{R*} + \frac{D_0}{2} m_{\tilde{\chi}_A^0} m_{\tilde{\chi}_B^0} N_{iBY}^L N_{iBX}^L N_{jAX}^{R*} N_{iAY}^{R*} \right] \quad (48)$$

$$e^2 B_4^{(n)L} = \frac{1}{16\pi^2} \left[\frac{D_0}{8} m_{\tilde{\chi}_A^0} m_{\tilde{\chi}_B^0} N_{jAX}^{R*} N_{iAY}^{R*} N_{iBY}^L N_{iBX}^L \right] \quad (49)$$

$$B_a^{(n)R} = B_a^{(n)L} \Big|_{L \leftrightarrow R} \quad a = 1, \dots, 4 \quad (50)$$

where

$$D_0 = D_0(m_{\tilde{\chi}_A^0}^2, m_{\tilde{\chi}_B^0}^2, m_{\tilde{l}_X}^2, m_{\tilde{l}_Y}^2) \quad (51)$$

$$\tilde{D}_0 = \tilde{D}_0(m_{\tilde{\chi}_A^0}^2, m_{\tilde{\chi}_B^0}^2, m_{\tilde{l}_X}^2, m_{\tilde{l}_Y}^2) \quad (52)$$

The chargino contributions read,

$$e^2 B_1^{(c)L} = \frac{1}{16\pi^2} \left[\frac{\tilde{D}_0}{2} C_{iAY}^R C_{jAX}^{R*} C_{iBX}^R C_{iBY}^{R*} \right] \quad (53)$$

$$e^2 B_2^{(c)L} = \frac{1}{16\pi^2} \left[\frac{\tilde{D}_0}{4} C_{iAY}^R C_{jAX}^{R*} C_{iBX}^L C_{iBY}^{L*} - \frac{D_0}{2} m_{\tilde{\chi}_A^-} m_{\tilde{\chi}_B^-} C_{iAY}^L C_{jAX}^{R*} C_{iBX}^R C_{iBY}^{L*} \right] \quad (54)$$

$$e^2 B_3^{(c)L} = \frac{1}{16\pi^2} \left[D_0 m_{\tilde{\chi}_A^-} m_{\tilde{\chi}_B^-} C_{iAY}^L C_{jAX}^{R*} C_{iBX}^L C_{iBY}^{R*} \right] \quad (55)$$

$$e^2 B_4^{(c)L} = 0 \quad (56)$$

$$B_a^{(c)R} = B_a^{(c)L} \Big|_{L \leftrightarrow R} \quad a = 1, \dots, 4 \quad (57)$$

where

$$D_0 = D_0(m_{\tilde{\chi}_A^-}^2, m_{\tilde{\chi}_B^-}^2, m_{\tilde{\nu}_X}^2, m_{\tilde{\nu}_Y}^2) \quad (58)$$

$$\tilde{D}_0 = \tilde{D}_0(m_{\tilde{\chi}_A^-}^2, m_{\tilde{\chi}_B^-}^2, m_{\tilde{\nu}_X}^2, m_{\tilde{\nu}_Y}^2) \quad (59)$$

D. The Higgs-penguin contributions

The diagrams where a Higgs boson is exchanged are called the Higgs-penguin diagrams. These are shown in fig. 4 and have been computed here by the first time. These are usually not considered in the literature. In particular, in the most complete study so far of [10] these Higgs-penguin diagrams were not included. However, they are expected to be relevant at large $\tan \beta$ [13]. We will therefore include them here. Specifically, we include the contributions from the three neutral MSSM Higgs bosons, h_0 , H_0 and A_0 and consider all SUSY loops.

In this case, the amplitude can be written as,

$$\begin{aligned} T_{\text{Higgs}} &= e^2 B_{2,\text{Higgs}}^L \{ [\bar{u}_i(p_1) (\gamma^\mu P_L) u_j(p)] [\bar{u}_i(p_2) (\gamma_\mu P_R) v_i(p_3)] - (p_1 \leftrightarrow p_2) \} \\ &+ e^2 B_{2,\text{Higgs}}^R \{ [\bar{u}_i(p_1) (\gamma^\mu P_R) u_j(p)] [\bar{u}_i(p_2) (\gamma_\mu P_L) v_i(p_3)] - (p_1 \leftrightarrow p_2) \} \\ &+ e^2 B_{3,\text{Higgs}}^L \{ [\bar{u}_i(p_1) P_L u_j(p)] [\bar{u}_i(p_2) P_L v_i(p_3)] - (p_1 \leftrightarrow p_2) \} \\ &+ e^2 B_{3,\text{Higgs}}^R \{ [\bar{u}_i(p_1) P_R u_j(p)] [\bar{u}_i(p_2) P_R v_i(p_3)] - (p_1 \leftrightarrow p_2) \} \end{aligned} \quad (60)$$

where

$$B_{a,\text{Higgs}}^{L,R} = B_{a,\text{Higgs}}^{(n)L,R} + B_{a,\text{Higgs}}^{(c)L,R} \quad a = 2, 3 \quad (61)$$

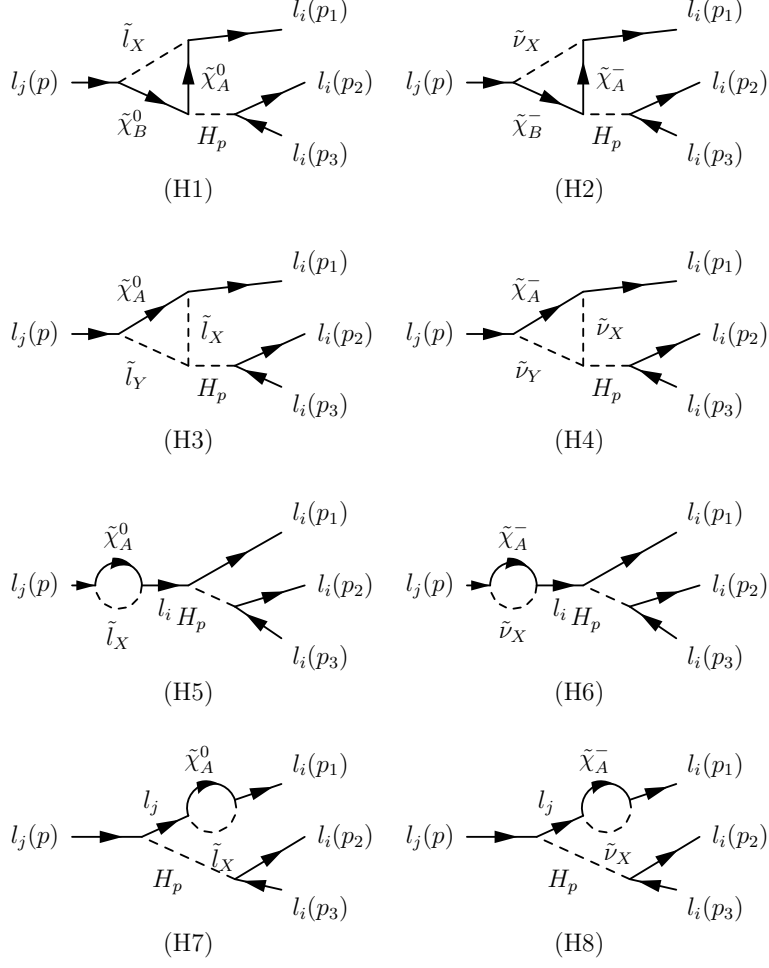


FIG. 4: Higgs-penguin diagrams contributing to the $l_j^- \rightarrow l_i^- l_i^- l_i^+$ decay. Here $H_p(p = 1, 2, 3) = h^0, H^0, A^0$.

The first term represents the neutralino contribution, which we find to be

$$e^2 B_{2,\text{Higgs}}^{(n)L} = \sum_{p=1}^3 \left(-\frac{1}{2} \right) \frac{1}{m_{H_p}^2} H_{L,n}^{(p)} S_{R,i}^{(p)} \quad (62)$$

$$e^2 B_{3,\text{Higgs}}^{(n)L} = \sum_{p=1}^3 \frac{1}{m_{H_p}^2} H_{L,n}^{(p)} S_{L,i}^{(p)} \quad (63)$$

$$B_{a,\text{Higgs}}^{(n)R} = B_{a,\text{Higgs}}^{(n)L} \Big|_{L \leftrightarrow R} \quad a = 2, 3 \quad (64)$$

where $H_p(p = 1, 2, 3) = h^0, H^0, A^0$ and

$$\begin{aligned}
H_{L,n}^{(p)} = & -\frac{1}{16\pi^2} \left\{ \left[B_0(m_{\tilde{\chi}_A^0}^2, m_{\tilde{\chi}_B^0}^2) + m_{\tilde{l}_X}^2 C_0(m_{\tilde{l}_X}^2, m_{\tilde{\chi}_A^0}^2, m_{\tilde{\chi}_B^0}^2) + m_{\tilde{l}_j}^2 C_{12}(m_{\tilde{l}_X}^2, m_{\tilde{\chi}_A^0}^2, m_{\tilde{\chi}_B^0}^2) \right. \right. \\
& + m_{\tilde{l}_i}^2 (C_{11} - C_{12})(m_{\tilde{l}_X}^2, m_{\tilde{\chi}_A^0}^2, m_{\tilde{\chi}_B^0}^2) \left. \right] N_{iAX}^L D_{R,AB}^{(p)} N_{jBX}^{R*} \\
& + m_{\tilde{l}_i} m_{\tilde{l}_j} (C_{11} + C_0)(m_{\tilde{l}_X}^2, m_{\tilde{\chi}_A^0}^2, m_{\tilde{\chi}_B^0}^2) N_{iAX}^R D_{L,AB}^{(p)} N_{jBX}^{L*} \\
& + m_{\tilde{l}_i} m_{\tilde{\chi}_B^0} (C_{11} - C_{12} + C_0)(m_{\tilde{l}_X}^2, m_{\tilde{\chi}_A^0}^2, m_{\tilde{\chi}_B^0}^2) N_{iAX}^R D_{L,AB}^{(p)} N_{jBX}^{R*} \\
& + m_{\tilde{l}_j} m_{\tilde{\chi}_B^0} C_{12}(m_{\tilde{l}_X}^2, m_{\tilde{\chi}_A^0}^2, m_{\tilde{\chi}_B^0}^2) N_{iAX}^L D_{R,AB}^{(p)} N_{jBX}^{L*} \\
& + m_{\tilde{l}_i} m_{\tilde{\chi}_A^0} (C_{11} - C_{12})(m_{\tilde{l}_X}^2, m_{\tilde{\chi}_A^0}^2, m_{\tilde{\chi}_B^0}^2) N_{iAX}^R D_{R,AB}^{(p)} N_{jBX}^{R*} \\
& + m_{\tilde{l}_j} m_{\tilde{\chi}_A^0} (C_{12} + C_0)(m_{\tilde{l}_X}^2, m_{\tilde{\chi}_A^0}^2, m_{\tilde{\chi}_B^0}^2) N_{iAX}^L D_{L,AB}^{(p)} N_{jBX}^{L*} \\
& + m_{\tilde{\chi}_A^0} m_{\tilde{\chi}_B^0} C_0(m_{\tilde{l}_X}^2, m_{\tilde{\chi}_A^0}^2, m_{\tilde{\chi}_B^0}^2) N_{iAX}^L D_{L,AB}^{(p)} N_{jBX}^{R*} \\
& + G_{XY}^{(p)\tilde{l}} \left[-m_{\tilde{l}_i} (C_{11} - C_{12})(m_{\tilde{\chi}_A^0}^2, m_{\tilde{l}_X}^2, m_{\tilde{l}_Y}^2) N_{iAX}^R N_{jAY}^{R*} \right. \\
& - m_{\tilde{l}_j} C_{12}(m_{\tilde{\chi}_A^0}^2, m_{\tilde{l}_X}^2, m_{\tilde{l}_Y}^2) N_{iAX}^L N_{jAY}^{L*} + m_{\tilde{\chi}_A^0} C_0(m_{\tilde{\chi}_A^0}^2, m_{\tilde{l}_X}^2, m_{\tilde{l}_Y}^2) N_{iAX}^L N_{jAY}^{R*} \left. \right] \\
& + \frac{S_{L,j}^{(p)}}{m_{\tilde{l}_i}^2 - m_{\tilde{l}_j}^2} \left[-m_{\tilde{l}_i}^2 B_1(m_{\tilde{\chi}_A^0}^2, m_{\tilde{l}_X}^2) N_{iAX}^L N_{jAX}^{L*} + m_{\tilde{l}_i} m_{\tilde{\chi}_A^0} B_0(m_{\tilde{\chi}_A^0}^2, m_{\tilde{l}_X}^2) N_{iAX}^R N_{jAX}^{L*} \right. \\
& - m_{\tilde{l}_i} m_{\tilde{l}_j} B_1(m_{\tilde{\chi}_A^0}^2, m_{\tilde{l}_X}^2) N_{iAX}^R N_{jAX}^{R*} + m_{\tilde{l}_j} m_{\tilde{\chi}_A^0} B_0(m_{\tilde{\chi}_A^0}^2, m_{\tilde{l}_X}^2) N_{iAX}^L N_{jAX}^{R*} \left. \right] \\
& + \frac{S_{L,i}^{(p)}}{m_{\tilde{l}_j}^2 - m_{\tilde{l}_i}^2} \left[-m_{\tilde{l}_j}^2 B_1(m_{\tilde{\chi}_A^0}^2, m_{\tilde{l}_X}^2) N_{iAX}^R N_{jAX}^{R*} + m_{\tilde{l}_j} m_{\tilde{\chi}_A^0} B_0(m_{\tilde{\chi}_A^0}^2, m_{\tilde{l}_X}^2) N_{iAX}^R N_{jAX}^{L*} \right. \\
& - m_{\tilde{l}_i} m_{\tilde{l}_j} B_1(m_{\tilde{\chi}_A^0}^2, m_{\tilde{l}_X}^2) N_{iAX}^L N_{jAX}^{L*} + m_{\tilde{l}_i} m_{\tilde{\chi}_A^0} B_0(m_{\tilde{\chi}_A^0}^2, m_{\tilde{l}_X}^2) N_{iAX}^L N_{jAX}^{R*} \left. \right] \left. \right\} \quad (65)
\end{aligned}$$

$$H_{R,n}^{(p)} = H_{L,n}^{(p)} \Big|_{L \leftrightarrow R} \quad p = 1, 2, 3 \quad (66)$$

The values of the couplings are given again in Appendix A and the loop functions in Appendix B. Correspondingly, the result for the chargino contribution is given by,

$$e^2 B_{2,\text{Higgs}}^{(c)L} = \sum_{p=1}^3 \left(-\frac{1}{2} \right) \frac{1}{m_{H_p}^2} H_{L,c}^{(p)} S_{R,i}^{(p)} \quad (67)$$

$$e^2 B_{3,\text{Higgs}}^{(c)L} = \sum_{p=1}^3 \frac{1}{m_{H_p}^2} H_{L,c}^{(p)} S_{L,i}^{(p)} \quad (68)$$

$$B_{a,\text{Higgs}}^{(c)R} = B_{a,\text{Higgs}}^{(c)L} \Big|_{L \leftrightarrow R} \quad a = 2, 3 \quad (69)$$

where $H_{L(R),c}^{(p)}$ can be obtained from the previous $H_{L(R),n}^{(p)}$ by replacing everywhere

$$\begin{aligned}\tilde{l} &\rightarrow \tilde{\nu} \\ \tilde{\chi}^0 &\rightarrow \tilde{\chi}^- \\ N^{L(R)} &\rightarrow C^{L(R)} \\ D_{L(R)} &\rightarrow W_{L(R)}\end{aligned}$$

Again the values of the couplings and the loop functions are given in Appendices A and B respectively.

E. $l_j^- \rightarrow l_i^- l_i^- l_i^+$ decay width

The decay width for $l_j^- \rightarrow l_i^- l_i^- l_i^+$ can be written in terms of the form factors given in the previous sections as [10]:

$$\begin{aligned}\Gamma(l_j^- \rightarrow l_i^- l_i^- l_i^+) &= \frac{e^4}{512\pi^3} m_{l_j}^5 \left[|A_1^L|^2 + |A_1^R|^2 - 2(A_1^L A_2^{R*} + A_2^L A_1^{R*} + h.c.) \right. \\ &+ \left(|A_2^L|^2 + |A_2^R|^2 \right) \left(\frac{16}{3} \log \frac{m_{l_j}}{m_{l_i}} - \frac{22}{3} \right) \\ &+ \frac{1}{6} \left(|B_1^L|^2 + |B_1^R|^2 \right) + \frac{1}{3} \left(|\hat{B}_2^L|^2 + |\hat{B}_2^R|^2 \right) \\ &+ \frac{1}{24} \left(|\hat{B}_3^L|^2 + |\hat{B}_3^R|^2 \right) + 6 \left(|B_4^L|^2 + |B_4^R|^2 \right) \\ &- \frac{1}{2} \left(\hat{B}_3^L B_4^{L*} + \hat{B}_3^R B_4^{R*} + h.c. \right) \\ &+ \frac{1}{3} \left(A_1^L B_1^{L*} + A_1^R B_1^{R*} + A_1^L \hat{B}_2^{L*} + A_1^R \hat{B}_2^{R*} + h.c. \right) \\ &- \frac{2}{3} \left(A_2^R B_1^{L*} + A_2^L B_1^{R*} + A_2^L \hat{B}_2^{R*} + A_2^R \hat{B}_2^{L*} + h.c. \right) \\ &+ \frac{1}{3} \left\{ 2 \left(|F_{LL}|^2 + |F_{RR}|^2 \right) + |F_{LR}|^2 + |F_{RL}|^2 \right. \\ &+ \left(B_1^L F_{LL}^* + B_1^R F_{RR}^* + \hat{B}_2^L F_{LR}^* + \hat{B}_2^R F_{RL}^* + h.c. \right) \\ &+ 2 \left(A_1^L F_{LL}^* + A_1^R F_{RR}^* + h.c. \right) + \left(A_1^L F_{LR}^* + A_1^R F_{RL}^* + h.c. \right) \\ &\left. - 4 \left(A_2^R F_{LL}^* + A_2^L F_{RR}^* + h.c. \right) - 2 \left(A_2^L F_{RL}^* + A_2^R F_{LR}^* + h.c. \right) \right\} \end{aligned} \tag{70}$$

where

$$F_{LL} = \frac{F_L Z_L^{(l)}}{g^2 \sin^2 \theta_W m_Z^2} \quad (71)$$

$$F_{RR} = F_{LL}|_{L \leftrightarrow R} \quad (72)$$

$$F_{LR} = \frac{F_L Z_R^{(l)}}{g^2 \sin^2 \theta_W m_Z^2} \quad (73)$$

$$F_{RL} = F_{LR}|_{L \leftrightarrow R} \quad (74)$$

Notice that we have put the Higgs contributions together with the box ones in order to follow closely the way of presentation of [10]

$$\hat{B}_2^{L,R} = B_2^{L,R} + B_{2,\text{Higgs}}^{L,R} \quad (75)$$

$$\hat{B}_3^{L,R} = B_3^{L,R} + B_{3,\text{Higgs}}^{L,R} \quad (76)$$

Notice that we have corrected the result in ref.[10] for the term that goes with $(|A_2^L| + |A_2^R|)$.

V. NUMERICAL RESULTS FOR THE LFV BRANCHING RATIOS

We present in this section the numerical results for all the branching ratios of LFV τ and μ decays in the context of the mSUGRA-seesaw scenario that has been introduced in the previous sections. We focus on the following LFV decays, $\tau^- \rightarrow \mu^- \mu^- \mu^+$, $\tau^- \rightarrow e^- e^- e^+$ and $\mu^- \rightarrow e^- e^- e^+$, and the radiative decays $\tau^- \rightarrow \mu^- \gamma$, $\tau^- \rightarrow e^- \gamma$ and $\mu^- \rightarrow e^- \gamma$. The reason to consider these radiative decays together with the decays into three leptons is that there are interesting correlations among them that provide additional information in testing SUSY. Specifically, we show in this section the correlations between the ratios of $\tau^- \rightarrow \mu^- \mu^- \mu^+$ and $\tau^- \rightarrow \mu^- \gamma$; between $\tau^- \rightarrow e^- e^- e^+$ and $\tau^- \rightarrow e^- \gamma$; and between $\mu^- \rightarrow e^- e^- e^+$ and $\mu^- \rightarrow e^- \gamma$. For the numerical estimates of the radiative decays we use the formula of [10], which is given in terms of the $A_2^{L,R}$ as,

$$\Gamma(l_j^- \rightarrow l_i^- \gamma) = \frac{e^2}{16\pi} m_{l_j}^5 (|A_2^L|^2 + |A_2^R|^2) \quad (77)$$

but we use our expressions for the form factors in eqs.(32), (33), (35) and (36) that include the lepton mass contributions. We explore here in full detail the size of the SUSY contributions to all these LFV $l_j \rightarrow 3l_i$ and $l_j \rightarrow l_i \gamma$ decays as a function of all the mSUGRA parameters, M_0 , $M_{1/2}$, A_0 , $\tan \beta$ and $\text{sign}(\mu)$ and the seesaw parameters m_{N_i} , $i = 1, 2, 3$ and R or,

equivalently, θ_1 , θ_2 and θ_3 . In all this numerical analysis we require compatibility with the neutrino data and with the present upper experimental bounds for all these branching ratios [5, 6, 7, 8, 9], as given explicitly in the introduction. We also demand the complete set of SUSY particle masses, which we derive with the SPheno program, to be above the present experimental lower bounds [20]. The numerical values of the total τ and μ widths (lifetimes) are taken from [20]. We show first the results for the scenario A with quasi-degenerate light and degenerate heavy neutrinos and next the most interesting scenario B with hierarchical light and hierarchical heavy neutrinos.

A. Degenerate case

We show in figs. 5 through 8 the numerical results of the branching ratios for the LFV τ and μ decays in scenario A with degenerate heavy neutrinos of mass m_N . We show our predictions for the three channels, $\tau^- \rightarrow \mu^- \mu^- \mu^+$, $\tau^- \rightarrow e^- e^- e^+$ and $\mu^- \rightarrow e^- e^- e^+$, and similarly, for the comparison with the leptonic radiative decays, $l_j \rightarrow l_i \gamma$, we also show in the plots the correlated decay, $\tau^- \rightarrow \mu^- \gamma$, $\tau^- \rightarrow e^- \gamma$ and $\mu^- \rightarrow e^- \gamma$, respectively.

The results of the branching ratios for the $\tau^- \rightarrow \mu^- \mu^- \mu^+$ and $\tau^- \rightarrow \mu^- \gamma$ decays as a function of $\tan \beta$ are illustrated in fig. 5. In these plots we set $m_N = 10^{14}$ GeV and assume the matrix R to be real. Notice that in the degenerate case with real R these LFV ratios do not depend on the particular choice for R . This can be easily understood because the dependence on R drops in the relevant factor, $(Y_\nu^* Y_\nu^T)_{ij}$, appearing in the dominant δ_{LL}^{ij} slepton mixing, and due to the property $R^T R = 1$. From this figure we also see that the predicted rates for both channels are well below their respective experimental upper bounds for all $\tan \beta$ values, eventhough the total rates grow fast with $\tan \beta$. We also see clearly the mentioned correlation between the $\tau^- \rightarrow \mu^- \mu^- \mu^+$ and $\tau^- \rightarrow \mu^- \gamma$ rates. In fact, this correlation is an immediate consequence of the dominance of the γ -penguin contributions which clearly governs the size of the $\tau^- \rightarrow \mu^- \mu^- \mu^+$ rates. This dominance is illustrated in fig. 5.(a). where the various contributions are shown separately. In fact, the contributions from the γ -penguin diagrams are almost undistinguishable from the total rates for all $\tan \beta$ values. For low $\tan \beta$ values the next dominant contribution is from the Z -penguin diagrams, but this is still more than one order of magnitude smaller than the γ -penguin contribution. The contributions from the box diagrams are even smaller. We

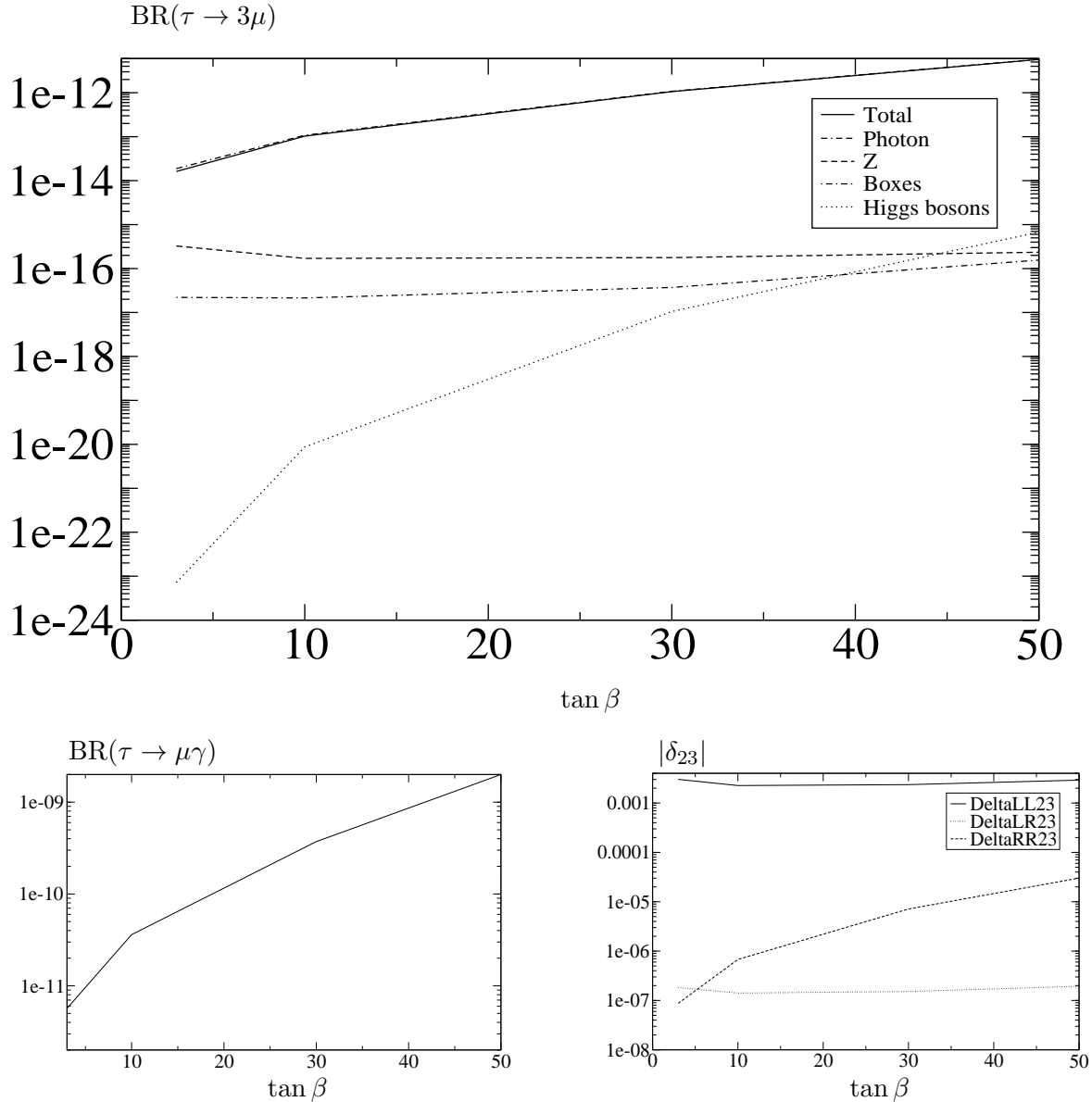


FIG. 5: Dependence of LVF τ decays with $\tan \beta$ in scenario A with degenerate heavy neutrinos and real R, for $m_N = 10^{14}$ GeV. (a) Upper panel, $BR(\tau \rightarrow \mu^- \mu^- \mu^+)$ and its different contributions, (b) lower-left panel, $BR(\tau \rightarrow \mu\gamma)$ and (c) lower-right panel, $|\delta_{LL,LR,RR}^{23}|$. The other input parameters are, $M_0 = 400$ GeV, $M_{1/2} = 300$ GeV, $A_0 = 0$ and $\text{sign}(\mu) > 0$.

also learn that the Z and boxes contributions do not depend significantly on $\tan \beta$, while the photon contribution goes approximately as $(\tan \beta)^2$ at large $\tan \beta$. In this large $\tan \beta$ region it is interesting to note that the total Higgs contribution becomes larger than the Z contribution and the boxes, due to the fact that it grows approximately as $(\tan \beta)^6$. In this total Higgs contribution the dominant penguins are those with H_0 and A_0 exchanged,

which are several orders of magnitude larger than the h_0 -penguin contribution. However, in spite of this huge enhancement of the total Higgs contribution occurring at large $\tan\beta$, its relative size as compared to the photon-penguin contribution is still negligible. For instance, for the values set in this figure of $M_0 = 400$ GeV, $M_{1/2} = 300$ GeV, $A_0 = 0$, $\text{sign}\mu > 0$ and $m_N = 10^{14}$ GeV, the Higgs contribution is still four orders of magnitude smaller than the photon-penguin contribution at $\tan\beta = 50$. This set of values give rise to the following MSSM spectrum (we just specify here the relevant sectors),

$$\begin{aligned}
m_{\tilde{t}_1} &= 247 \text{ GeV} & m_{\tilde{\chi}_1^0} &= 121 \text{ GeV} & m_{h^0} &= 114 \text{ GeV} \\
m_{\tilde{t}_2} &= 397 \text{ GeV} & m_{\tilde{\chi}_2^0} &= 232 \text{ GeV} & m_{H^0} &= 457 \text{ GeV} \\
m_{\tilde{t}_3} &= 413 \text{ GeV} & m_{\tilde{\chi}_3^0} &= 484 \text{ GeV} & m_{A^0} &= 457 \text{ GeV} \\
m_{\tilde{t}_4} &= 416 \text{ GeV} & m_{\tilde{\chi}_4^0} &= 493 \text{ GeV} & m_{\tilde{\nu}_1} &= 351 \text{ GeV} \\
m_{\tilde{t}_5} &= 417 \text{ GeV} & m_{\tilde{\chi}_1^-} &= 232 \text{ GeV} & m_{\tilde{\nu}_2} &= 409 \text{ GeV} \\
m_{\tilde{t}_6} &= 419 \text{ GeV} & m_{\tilde{\chi}_2^-} &= 495 \text{ GeV} & m_{\tilde{\nu}_3} &= 410 \text{ GeV}.
\end{aligned}$$

We have checked that other choices of parameters, specially lower M_0 and $M_{1/2}$ lead to larger contributions from the Higgs penguins, since one gets lighter SUSY spectra and more importantly lighter H_0 and A_0 bosons. However, the present experimental lower bounds on the MSSM particle masses, do not allow to decrease much these M_0 and $M_{1/2}$ values, so that in this mSUGRA context the relevant m_{H_0} , and m_{A_0} masses can never get low enough values such that their corresponding Higgs-penguin contributions be competitive with the γ -penguin ones. From this figure we conclude then that the leading γ -penguin approximation works extremely well, for all $\tan\beta$ values. In this approximation one gets,

$$\frac{BR(l_j \rightarrow 3l_i)}{BR(l_j \rightarrow l_i\gamma)} = \frac{\alpha}{3\pi} \left(\log \frac{m_{l_j}^2}{m_{l_i}^2} - \frac{11}{4} \right) \quad (78)$$

which leads to the approximate values of $\frac{1}{440}$, $\frac{1}{94}$ and $\frac{1}{162}$ for $(l_j l_i) = (\tau\mu), (\tau e)$ and (μe) , respectively. As will be seen later it also works extremely well in the other channels. These nearly constant values of the ratios of branching ratios will be showing along this work. Obviously, if these ratios could be measured they could provide interesting information.

In fig. 5(c) we have included our predictions for $|\delta_{LL}^{23}|, |\delta_{LR}^{23}|$ and, $|\delta_{RR}^{23}|$, as defined in eqs.(24),(25) and (26) respectively, as a function of $\tan\beta$. These are the flavor changing parameters that are the relevant ones for the τ decays having μ in the final state. It is also interesting to compare them with the predictions in the leading logarithmic approximation

where the generated mixing in the off-diagonal terms ($i \neq j, i, j = 1, 2, 3$), through the running from M_X down to m_M , is given by

$$\begin{aligned}
(\Delta m_L^2)_{ij} &= -\frac{1}{8\pi^2}(3M_0^2 + A_0^2)(Y_\nu^* LY_\nu^T)_{ij} \\
(\Delta A_l)_{ij} &= -\frac{3}{16\pi^2}A_0 Y_{li}(Y_\nu^* LY_\nu^T)_{ij} \\
(\Delta m_E^2)_{ij} &= 0 ; L_{kl} \equiv \log\left(\frac{M_X}{m_{M_k}}\right) \delta_{kl}.
\end{aligned} \tag{79}$$

and, in consequence, it predicts the hierachy, $|\delta_{LL}^{23}| > |\delta_{LR}^{23}| > |\delta_{RR}^{23}|$.

As expected from the leading-log approximation, we see in fig. 5(c) that $|\delta_{LL}^{23}|$ is much larger than $|\delta_{LR}^{23}|$ and $|\delta_{RR}^{23}|$. However, we get $|\delta_{RR}^{23}|$ larger than $|\delta_{LR}^{23}|$ and it can be indeed two orders of magnitude larger than $|\delta_{LR}^{23}|$ at large $\tan\beta$. It is clear that, at least for our choice here of $A_0 = 0$, the leading-log approximation does not fully work. We also learn from this figure that the size of the mixing is always small in the degenerate case, being the largest $|\delta_{LL}^{23}|$ about 3×10^{-3} .

We next comment on the relevance of the choice for the m_N values. In fig. 6 we have illustrated the $\tau \rightarrow \mu^- \mu^- \mu^+$ and $\tau \rightarrow \mu \gamma$ branching ratios as a function of m_N for degenerate heavy neutrinos and $\tan\beta = 50$. The explored range in m_N is from 10^8 GeV up to 10^{14} GeV which is favorable for baryogenesis. Both rates have the same behaviour with m_N which corresponds approximately to $BR(\tau \rightarrow \mu^- \mu^- \mu^+)$, $BR(\tau \rightarrow \mu \gamma) \propto |m_N \log(m_N)|^2$. As before, these two predicted branching ratios are well below their experimental upper bounds, even at the largest m_N value of 10^{14} GeV. In the last plot of fig. 6 we include the dependence of $|\delta_{LL}^{23}|, |\delta_{LR}^{23}|, |\delta_{RR}^{23}|$ on m_N which clearly show a correlated behaviour with the previous plots. Again, $|\delta_{LL}^{23}|$ is the dominant one reaching values up to about 3×10^{-3} , and δ_{RR}^{23} is larger than δ_{LR}^{23} .

For completeness, we also include the results of the other four LFV τ and μ decays in fig. 7, where the predictions are shown as a function of $\tan\beta$. These behaviours are very similar to those in $BR(\tau^- \rightarrow \mu^- \mu^- \mu^+)$ and $BR(\tau \rightarrow \mu \gamma)$ decays correspondingly. The main difference is in the lower plots, where now $|\delta_{LR}^{12(13)}|$ is larger than $|\delta_{RR}^{12(13)}|$. The maximum reached values are very small in this case, $|\delta_{LL}^{12(13)}| \sim 5 \times 10^{-5}$. We see again that the leading γ -penguin approximation works extremely well for these channels, and the previously mentioned values of the ratios of branching ratios give a pretty good answer. We also find that the rates for all these four decays are well below their corresponding experimental bounds, in the degenerate

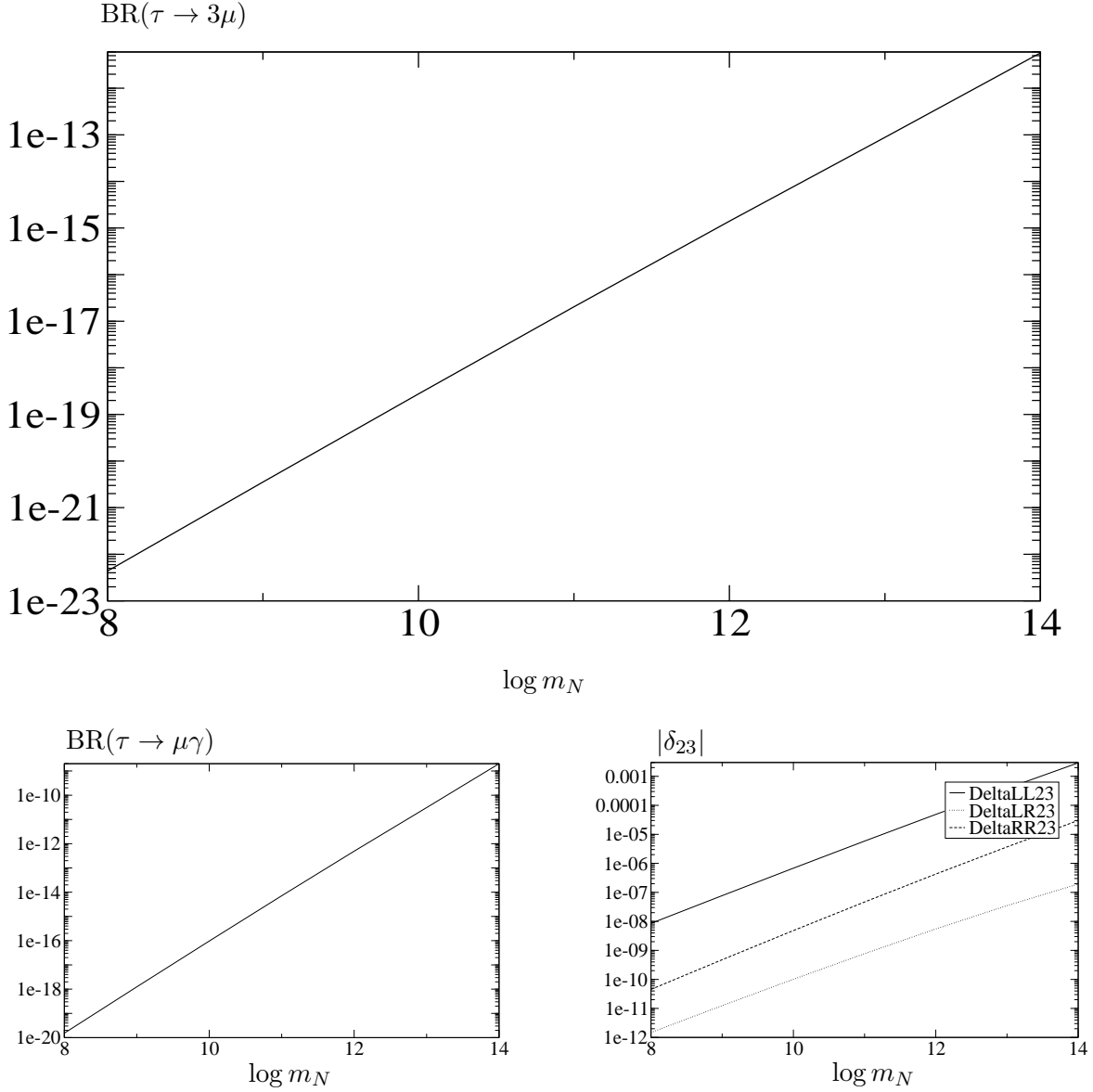


FIG. 6: Dependence of LFV τ decays with m_N in scenario A with degenerate heavy neutrinos and real R, for $\tan\beta = 50$. (a) Upper panel, $BR(\tau \rightarrow \mu^- \mu^- \mu^+)$, (b) lower-left panel, $BR(\tau \rightarrow \mu \gamma)$ and (c) lower-right panel, $|\delta_{LL,LR,RR}^{23}|$. The other input parameters are, $M_0 = 400$ GeV, $M_{1/2} = 300$ GeV, $A_0 = 0$ and $\text{sign}(\mu) > 0$.

case, for all the explored values of $\tan\beta$ and m_N .

To end up the study of the degenerate case, we have also explored the dependence of the largest ratios $BR(\tau^- \rightarrow \mu^- \mu^- \mu^+)$ and $BR(\tau^- \rightarrow \mu^- \gamma)$ with the mSUGRA parameters M_0 and $M_{1/2}$. These results are shown in fig 8. We see clearly a similar behaviour in the two channels and their rates decrease as expected when increasing the soft SUSY breaking

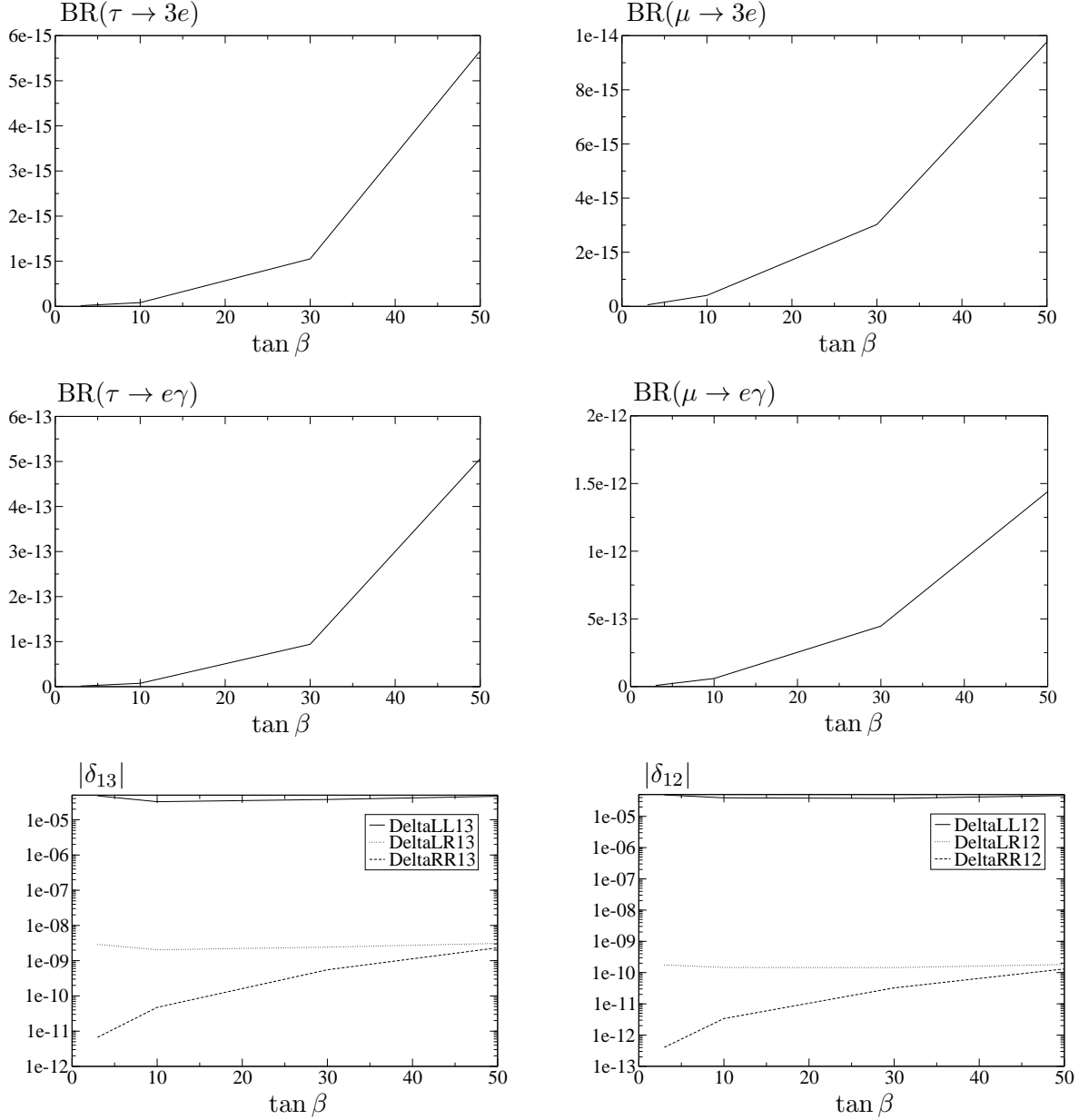


FIG. 7: Dependence of LFV τ and μ decays with $\tan \beta$ in scenario A with degenerate heavy neutrinos and real R, for $m_N = 10^{14}$ GeV. (a) Upper-left panel, $BR(\tau \rightarrow e^- e^- e^+)$, (b) upper-right panel, $BR(\mu \rightarrow e^- e^- e^+)$, (c) middle-left panel, $BR(\tau \rightarrow e\gamma)$, (d) middle-right panel, $BR(\mu \rightarrow e\gamma)$, (e) lower-left panel, $|\delta_{LL,LR,RR}^{13}|$ and (f) lower-right panel, $|\delta_{LL,LR,RR}^{12}|$. The other input parameters are, $M_0 = 400$ GeV, $M_{1/2} = 300$ GeV, $A_0 = 0$ and $\text{sign}(\mu) > 0$.

mass parameters. This implies that for large enough values of M_0 or $M_{1/2}$ the branching ratios are considerably suppressed, due to the decoupling of the heavy SUSY particles in the dominant loops which are common to both observables. Thus, looking at these plots we can obviously conclude that the lighter the SUSY spectrum is, the larger branching ratios we

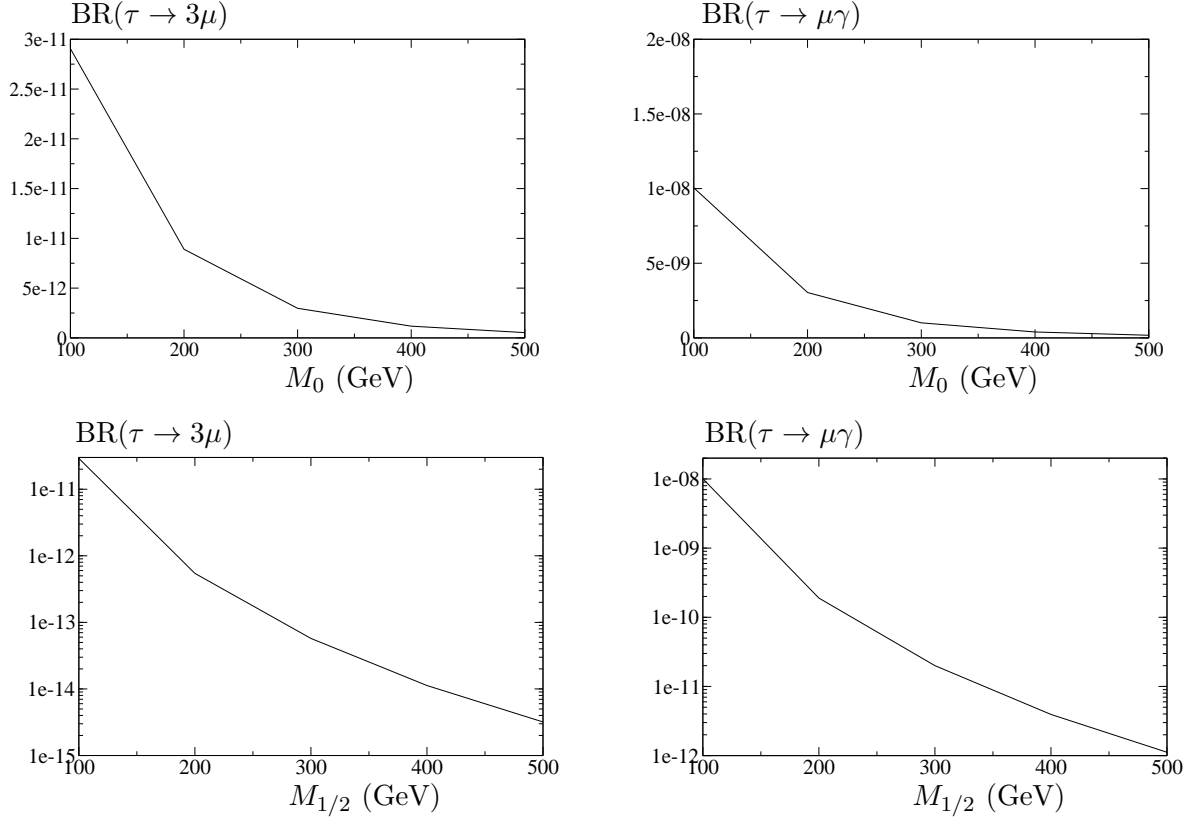


FIG. 8: Dependence of $BR(\tau^- \rightarrow \mu^- \mu^- \mu^+)$ and $BR(\tau \rightarrow \mu\gamma)$ with M_0 and $M_{1/2}$ in scenario A with degenerate heavy neutrinos and real R, for $m_N = 10^{14}$ GeV and $\tan\beta = 50$. (a) Upper-left panel, $BR(\tau \rightarrow \mu^- \mu^- \mu^+)$ as a function of M_0 for $M_{1/2} = 100$ GeV, (b) upper-right panel, $BR(\tau \rightarrow \mu\gamma)$ as a function of M_0 for $M_{1/2} = 100$ GeV, (c) lower-left panel, $BR(\tau \rightarrow \mu^- \mu^- \mu^+)$ as a function of $M_{1/2}$ for $M_0 = 100$ GeV, (d) lower-right panel, $BR(\tau \rightarrow \mu\gamma)$ as a function of $M_{1/2}$ for $M_0 = 100$ GeV. In all the plots we take $A_0 = 0$ and $\text{sign}(\mu) > 0$.

get. However, as already said, the more interesting region of low M_0 and/or $M_{1/2}$ values, being close to 100 GeV, is not allowed by the present experimental lower bounds on the MSSM particle masses.

In summary, in the case of degenerate heavy neutrinos, we get LFV τ and μ decay rates which are still below their present experimental upper bounds, for all the explored values of the seesaw and mSUGRA parameters, which have been required to provide a full MSSM spectrum with masses being compatible with the present experimental bounds.

B. Hierarchical case

We next present the results for hierarchical neutrinos, scenario B, which are much more promising. In this case the choice for R is very relevant. The results for the general complex R case and for the particular mass hierarchy $(m_{N_1}, m_{N_2}, m_{N_3}) = (10^8, 2 \times 10^8, 10^{14})$ GeV, are shown in figs. 9 through 14. This particular choice for the heavy neutrino masses seems to generate a proper rate for baryogenesis via leptogenesis in the hierarchical case [24]. We will later explore other choices as well.

From these figures we first confirm that the LFV τ and μ decay rates are much larger in the hierarchical case than in the degenerate one. This is true even for the case of real R , which corresponds in our plots to the predictions at $\arg(\theta_1) = \arg(\theta_2) = \arg(\theta_3) = 0$. Furthermore, we get severe restrictions on the maximum allowed decay rates coming from the experimental upper bounds.

The predictions for $BR(\tau^- \rightarrow \mu^- \mu^- \mu^+)$ and $BR(\tau \rightarrow \mu \gamma)$ as a function of $|\theta_2|$ are depicted in fig 9. Here θ_1 and θ_3 are set to zero, and $\arg(\theta_2) = \pi/4$. From now on the arguments of θ_1, θ_2 and θ_3 are written in radians. The other parameters are set to $\tan \beta = 50$, $M_0 = 400$ GeV, $M_{1/2} = 300$ GeV, $A_0 = 0$ and $\text{sign}(\mu) > 0$. In fig. 9(a) we show separately the various contributions to $BR(\tau^- \rightarrow \mu^- \mu^- \mu^+)$. The dominant one is again the photon-penguin contribution (which is undistinguishable from the total in this figure) and the others are several orders of magnitude smaller. We also see that the relative size of the subdominant contributions have changed respect to the previously studied degenerate case. Now the Higgs contribution is larger than the boxes one and this is larger than the Z one. This is so because the largest $\tan \beta = 50$ value has been set. All the rates for $\tau^- \rightarrow \mu^- \mu^- \mu^+$ in this plot are within the allowed range by the experimental bound, which is placed just at the upper line of the rectangle. In contrast, one can see in fig .9(b) that, for the chosen mSUGRA and seesaw parameters, the predicted $BR(\tau \rightarrow \mu \gamma)$ are clearly above the experimental bound. The dependence of $|\delta_{LL,LR,RR}^{23}|$ with $|\theta_2|$ is shown in fig. 9(c). We see that $|\delta_{LL}^{23}|$ can reach very large values, up to 0.4, for $|\theta_2| = 3$ and $\arg(\theta_2) = \pi/4$. We have checked that this particular choice of $\theta_2 = 3e^{i\pi/4}$ gives rise to large neutrino Yukawa matrix elements $|Y_\nu^{33}|$ and $|Y_\nu^{23}|$ of the order of 1, which are the responsible for this large mixing in the slepton sector.

It is also interesting to compare the MSSM spectrum for this hierarchical case with the

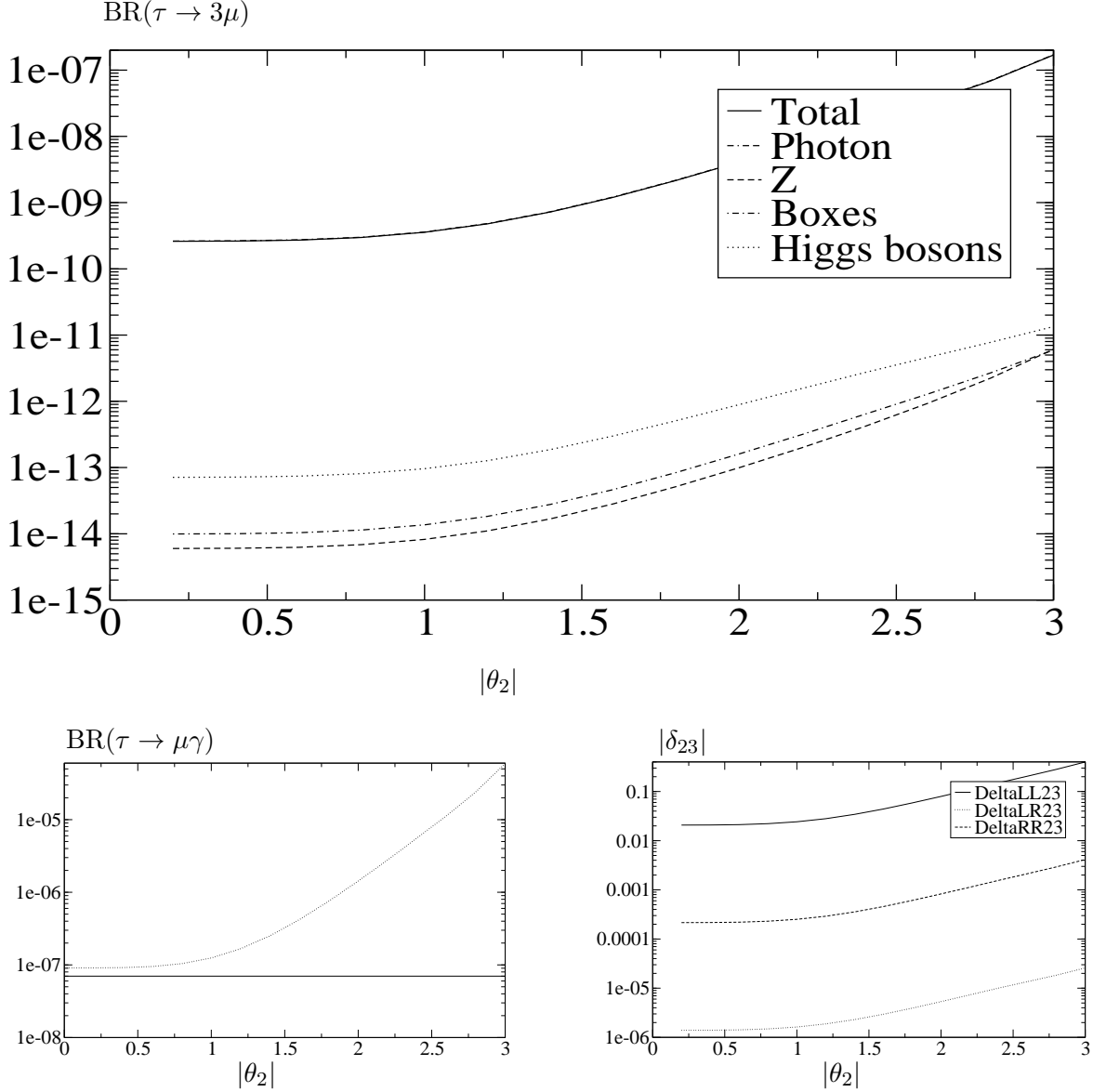


FIG. 9: (a) Upper panel: Dependence of $BR(\tau^- \rightarrow \mu^- \mu^- \mu^+)$ with $|\theta_2|$, (b) lower-left panel: Dependence of $BR(\tau \rightarrow \mu\gamma)$ with $|\theta_2|$, (c) lower right panel: $|\delta_{LL,LR,RR}^{23}|$ with $|\theta_2|$. The horizontal line is the upper experimental bound. All panels are in scenario B, for $\arg(\theta_2) = \pi/4$, $(m_{N_1}, m_{N_2}, m_{N_3}) = (10^8, 2 \times 10^8, 10^{14})$ GeV, $\theta_1 = \theta_3 = 0$, $\tan \beta = 50$, $M_0 = 400$ GeV, $M_{1/2} = 300$ GeV, $A_0 = 0$ and $\text{sign}(\mu) > 0$.

previous degenerate case. For the input values of fig. 9 but with θ_2 set to the extreme value $\theta_2 = 2.8e^{i\frac{\pi}{4}}$ we get the following masses,

$$\begin{aligned}
m_{\tilde{l}_1} &= 230 \text{ GeV} & m_{\tilde{\chi}_1^0} &= 122 \text{ GeV} & m_{h^0} &= 114 \text{ GeV} \\
m_{\tilde{l}_2} &= 356 \text{ GeV} & m_{\tilde{\chi}_2^0} &= 232 \text{ GeV} & m_{H^0} &= 455 \text{ GeV} \\
m_{\tilde{l}_3} &= 413 \text{ GeV} & m_{\tilde{\chi}_3^0} &= 481 \text{ GeV} & m_{A^0} &= 455 \text{ GeV} \\
m_{\tilde{l}_4} &= 417 \text{ GeV} & m_{\tilde{\chi}_4^0} &= 490 \text{ GeV} & m_{\tilde{\nu}_1} &= 296 \text{ GeV} \\
m_{\tilde{l}_5} &= 436 \text{ GeV} & m_{\tilde{\chi}_1^-} &= 232 \text{ GeV} & m_{\tilde{\nu}_2} &= 422 \text{ GeV} \\
m_{\tilde{l}_6} &= 448 \text{ GeV} & m_{\tilde{\chi}_2^-} &= 492 \text{ GeV} & m_{\tilde{\nu}_3} &= 441 \text{ GeV}
\end{aligned}$$

It is obvious that the complex R affects significantly the predictions of the MSSM masses, specially in the slepton sector. In general, the slepton mixing generated by the complex θ_i , lower the lightest charged slepton and the lightest sneutrino masses and increases the heaviest charged slepton and sneutrino masses.

In fig. 10 we show the predictions of $BR(l_j^- \rightarrow l_i^- l_i^- l_i^+)$ and $BR(l_j \rightarrow l_i \gamma)$ as functions of $|\theta_2|$, for all the channels and for the different values of $\arg(\theta_2) = 0, \pi/10, \pi/8, \pi/6, \pi/4$. In all these plots we set again $\tan\beta = 50$, $M_0 = 400 \text{ GeV}$, $M_{1/2} = 300 \text{ GeV}$, $A_0 = 0$, $\text{sign}(\mu) > 0$ and $(m_{N_1}, m_{N_2}, m_{N_3}) = (10^8, 2 \times 10^8, 10^{14}) \text{ GeV}$. The upper lines correspond to $\arg(\theta_2) = \pi/4$ and the lower ones to $\arg(\theta_2) = 0$. These lower lines are therefore the corresponding predictions for real R . It is clear that all the branching ratios have a soft behaviour with $|\theta_2|$ except for the case of real θ_2 where appears a narrow dip in each plot. In this fig. 10 we see that all the rates obtained are below their experimental upper bounds, except for the processes $\tau \rightarrow \mu \gamma$ and $\mu \rightarrow e \gamma$, where the predicted rates for complex θ_2 with large $|\theta_2|$ are clearly above the allowed region. The most restrictive channel in this case is $\tau \rightarrow \mu \gamma$ where compatibility with data occurs just for real θ_2 and for complex θ_2 but with $|\theta_2|$ values near the region of the narrow dip. We also see that the rates for $BR(\mu \rightarrow 3e)$ enter in conflict with experiment at the upper corner of large $|\theta_2|$ and large $\arg(\theta_2) = \pi/4$.

Even more interesting are the predictions for $BR(l_j^- \rightarrow l_i^- l_i^- l_i^+)$ and $BR(l_j \rightarrow l_i \gamma)$ as functions of $|\theta_1|$, due to the large values of the relevant entries of the Y_ν coupling matrix, which are illustrated in fig. 11. Concretely, $|Y_\nu^{13}|$ can be as large as ~ 0.2 for $|\theta_1| \sim 2.5$ and $\arg(\theta_1) = \pi/4$, and $|Y_\nu^{23}|$ and $|Y_\nu^{33}|$ are in the range $0.1 - 1$ for all studied complex θ_1 values. The results for $BR(l_j^- \rightarrow l_i^- l_i^- l_i^+)$ and $BR(l_j \rightarrow l_i \gamma)$ as functions of $|\theta_1|$, for different values of $\arg(\theta_1)$, are illustrated in fig. 12. Here θ_2 and θ_3 are set to zero. The same set of mSUGRA parameters and heavy neutrino masses as in fig. 10 are taken for comparison. We see clearly that the restrictions are more severe in this case than in the previous one. In fact, all the rates cross the horizontal lines of the experimental bounds except for $BR(\tau^- \rightarrow \mu^- \mu^- \mu^+)$

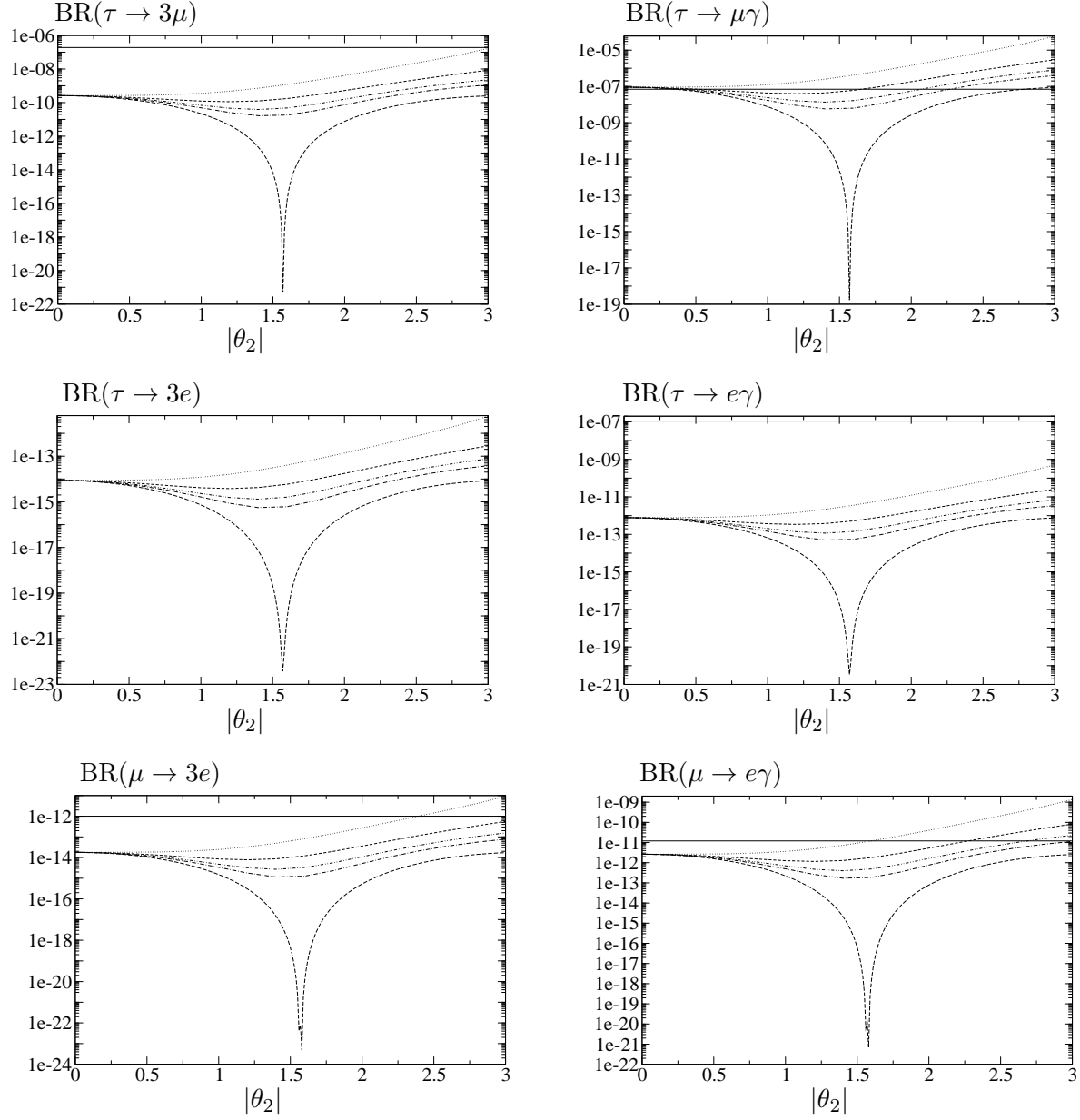


FIG. 10: Dependence of LFV τ and μ decays with $|\theta_2|$ in scenario B with hierarchical heavy neutrinos and complex R, for $\arg(\theta_2) = 0, \pi/10, \pi/8, \pi/6, \pi/4$ in radians (lower to upper lines), $(m_{N_1}, m_{N_2}, m_{N_3}) = (10^8, 2 \times 10^8, 10^{14})$ GeV, $\theta_1 = \theta_3 = 0$, $\tan \beta = 50$, $M_0 = 400$ GeV, $M_{1/2} = 300$ GeV, $A_0 = 0$ and $\text{sign}(\mu) > 0$. The horizontal lines are the upper experimental bounds.

and $BR(\tau^- \rightarrow e^- e^- e^+)$. The most restrictive channel is now the $\mu \rightarrow e\gamma$ decay. More specifically, we see that all the points in the plot of $BR(\mu \rightarrow e\gamma)$, except for the particular values $\theta_1 = 0$ and real θ_1 at the dip, are excluded by the experimental upper bound. Also the predictions for $BR(\mu \rightarrow 3e)$ are mostly excluded, except again for the region close to zero and the dip. Notice that the qualitative behaviour of these all branching ratios with $|\theta_1|$

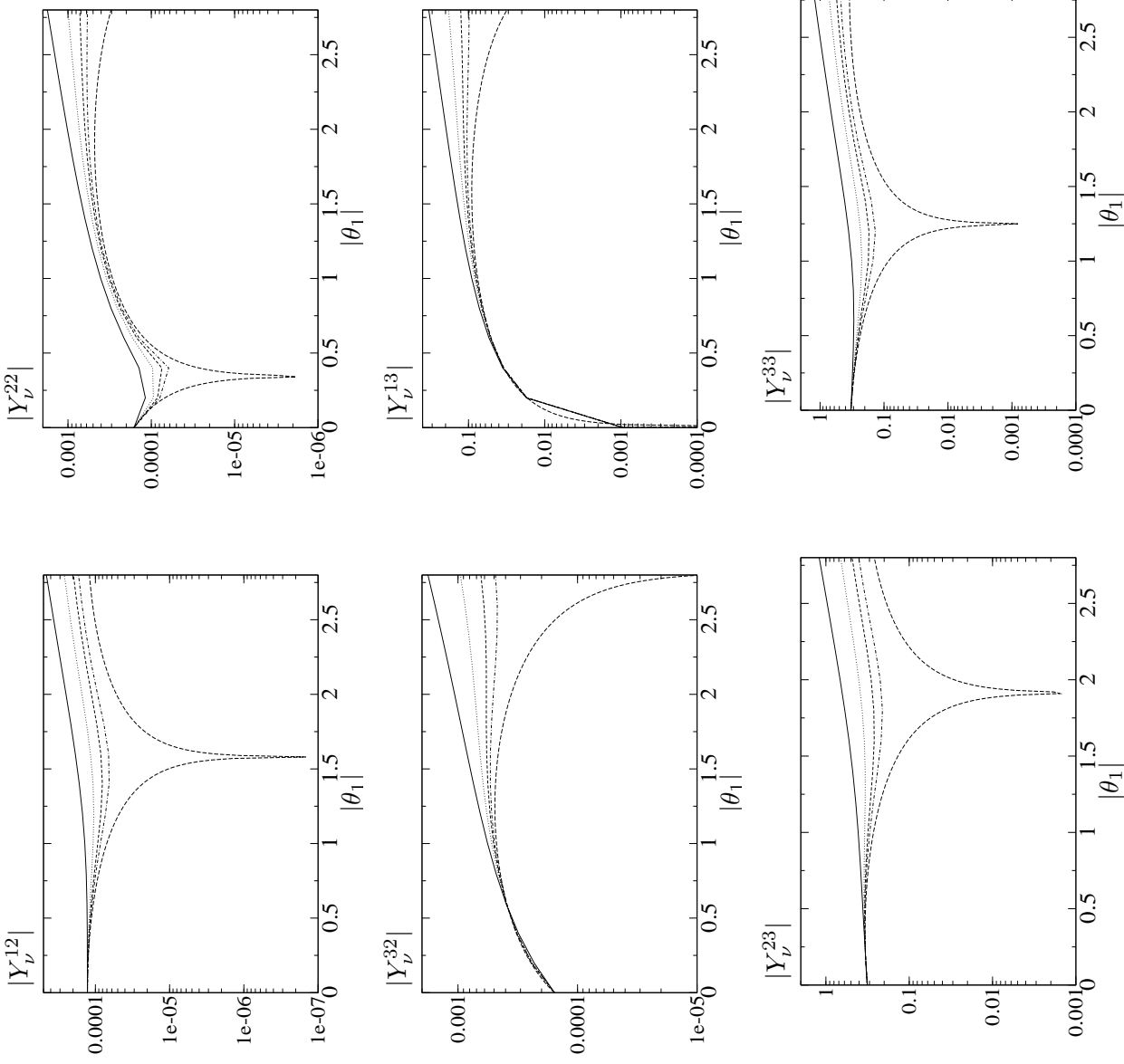


FIG. 11: Dependence of $|Y_{\nu}|$ with $|\theta_1|$ in scenario B with hierarchical heavy neutrinos and complex R, for $\arg(\theta_1) = 0, \pi/10, \pi/8, \pi/6, \pi/4$ in radians (lower to upper lines), $(m_{N_1}, m_{N_2}, m_{N_3}) = (10^8, 2 \times 10^8, 10^{14})$ GeV, $\theta_2 = \theta_3 = 0$, $\tan\beta = 50$, $M_0 = 400$ GeV, $M_{1/2} = 300$ GeV and $A_0 = 0$.

in fig. 12 and the locations of the dips can be explained from the Yukawa coupling matrix behaviour in fig. 11.

The scenario most seriously in conflict with experiment is shown in fig. 13 where the predictions for $BR(l_j^- \rightarrow l_i^- l_i^- l_i^+)$ and $BR(l_j^- \rightarrow l_i^- l_i^- l_i^+)$ are again plotted as a function of $|\theta_1|$ and for the same choices of $\arg(\theta_1)$ as in the previous case, but now the mSUGRA mass parameters are set to the lower values, $M_0 = 250$ GeV, and $M_{1/2} = 150$ GeV. These lead to

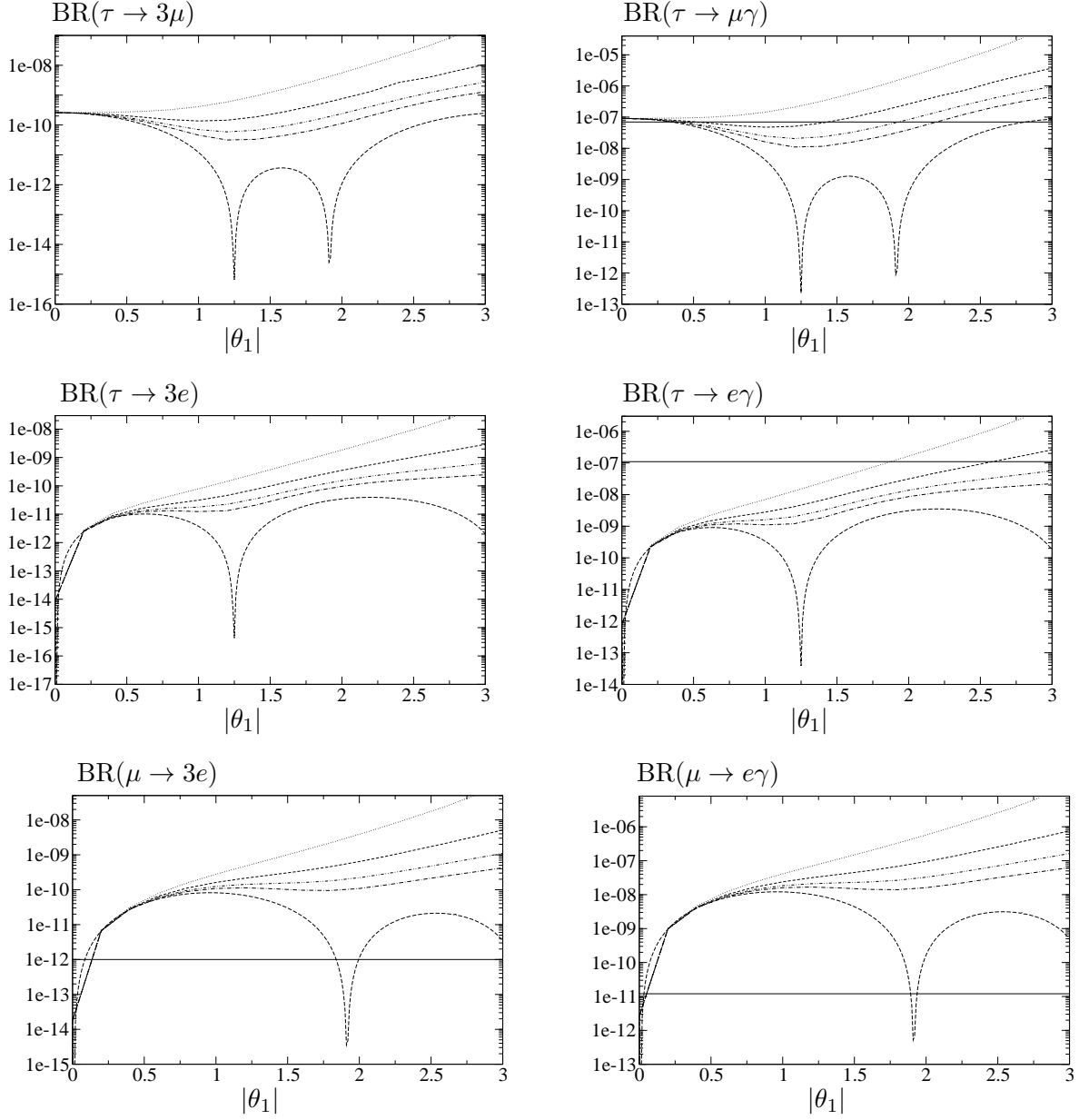


FIG. 12: Dependence of LFV τ and μ decays with $|\theta_1|$ in scenario B with hierarchical heavy neutrinos and complex R, for $\arg(\theta_1) = 0, \pi/10, \pi/8, \pi/6, \pi/4$ in radians (lower to upper lines), $(m_{N_1}, m_{N_2}, m_{N_3}) = (10^8, 2 \times 10^8, 10^{14})$ GeV, $\theta_2 = \theta_3 = 0$, $\tan \beta = 50$, $M_0 = 400$ GeV, $M_{1/2} = 300$ GeV and $A_0 = 0$. The horizontal lines are the upper experimental bounds.

a lighter MSSM spectrum and in consequence to higher rates. For comparison with the previous cases, we include below the predicted masses of the relevant MSSM particles, for the particular value $\theta_1 = 2.8e^{i\frac{\pi}{4}}$,

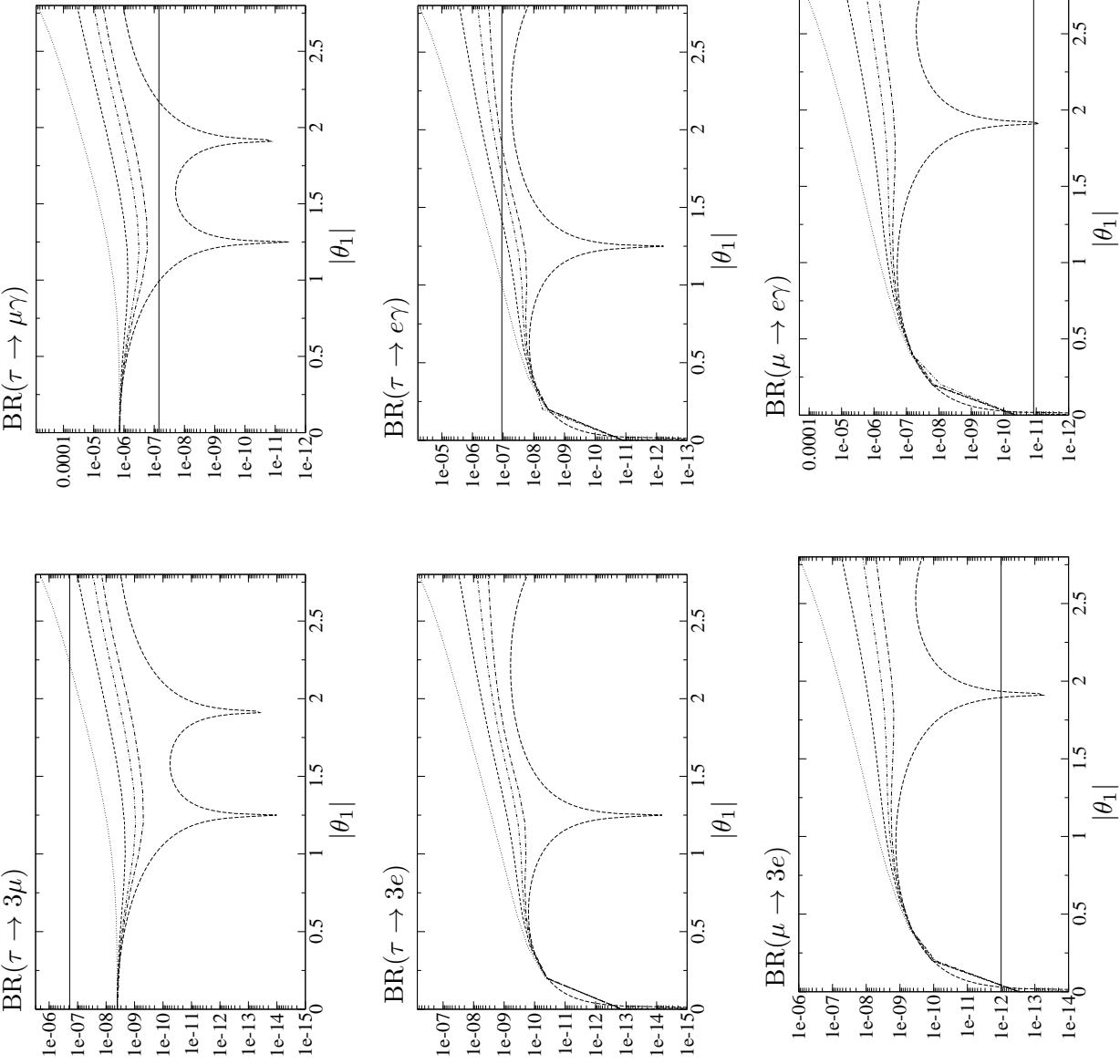


FIG. 13: Dependence of LFV τ and μ decays with $|\theta_1|$ in scenario B with hierarchical heavy neutrinos and complex R, for $\arg(\theta_1) = 0, \pi/10, \pi/8, \pi/6, \pi/4$ in radians (lower to upper lines), ($m_{N_1}, m_{N_2}, m_{N_3}$) = $(10^8, 2 \times 10^8, 10^{14})$ GeV, $\theta_2 = \theta_3 = 0$, $\tan \beta = 50$, $M_0 = 250$ GeV, $M_{1/2} = 150$ GeV and $A_0 = 0$. The horizontal lines are the upper experimental bounds.

$$\begin{aligned}
m_{\tilde{l}_1} &= 94 \text{ GeV} & m_{\tilde{\chi}_1^0} &= 58 \text{ GeV} & m_{h^0} &= 108 \text{ GeV} \\
m_{\tilde{l}_2} &= 218 \text{ GeV} & m_{\tilde{\chi}_2^0} &= 107 \text{ GeV} & m_{H^0} &= 269 \text{ GeV} \\
m_{\tilde{l}_3} &= 259 \text{ GeV} & m_{\tilde{\chi}_3^0} &= 284 \text{ GeV} & m_{A^0} &= 269 \text{ GeV} \\
m_{\tilde{l}_4} &= 259 \text{ GeV} & m_{\tilde{\chi}_4^0} &= 296 \text{ GeV} & m_{\tilde{\nu}_1} &= 143 \text{ GeV} \\
m_{\tilde{l}_5} &= 273 \text{ GeV} & m_{\tilde{\chi}_1^-} &= 107 \text{ GeV} & m_{\tilde{\nu}_2} &= 247 \text{ GeV} \\
m_{\tilde{l}_6} &= 273 \text{ GeV} & m_{\tilde{\chi}_2^-} &= 300 \text{ GeV} & m_{\tilde{\nu}_3} &= 261 \text{ GeV}
\end{aligned}$$

Notice that the lightest slepton, neutralino, chargino and Higgs boson have masses close to their experimental lower bounds.

We conclude from this fig. 13 that the predictions for $BR(\mu \rightarrow e\gamma)$ and $BR(\mu \rightarrow 3e)$ are totally excluded by present data and the predictions for $BR(\tau \rightarrow \mu\gamma)$ are practically excluded, with the exception of the two narrow dips. The predictions for $BR(\tau \rightarrow e\gamma)$ get severe restrictions for complex θ_1 with large $|\theta_1|$ and/or large $\arg(\theta_1)$, and the rates for $BR(\tau \rightarrow 3\mu)$ start being sensitive to the present experimental bounds for large complex θ_1 values in the upper corner of the plot.

We have also explored the dependence with the complex θ_3 angle, and it turns out that the predictions for all rates are nearly constant with this angle. For instance, for $\tan\beta = 50$, $M_0 = 400 \text{ GeV}$, $M_{1/2} = 300 \text{ GeV}$, $A_0 = 0$ and $\text{sign}(\mu) > 0$, we get $BR(\tau \rightarrow 3\mu) = 2.6 \times 10^{-10}$, $BR(\tau \rightarrow 3e) = 8.8 \times 10^{-15}$, $BR(\mu \rightarrow 3e) = 1.8 \times 10^{-14}$, $BR(\tau \rightarrow \mu\gamma) = 9.1 \times 10^{-8}$, $BR(\tau \rightarrow e\gamma) = 7.8 \times 10^{-13}$ and $BR(\mu \rightarrow e\gamma) = 2.6 \times 10^{-12}$. In this case only the prediction for $BR(\tau \rightarrow \mu\gamma)$ is in conflict with the experiment.

The dependence of $BR(\tau^- \rightarrow \mu^- \mu^- \mu^+)$ and $BR(\tau \rightarrow \mu\gamma)$ with the mSUGRA parameters M_0 and $M_{1/2}$ is illustrated in fig. 14. We see a similar behaviour as in the degenerate case, where a suppression of the branching ratios occurs for large values of M_0 and/or $M_{1/2}$. Whereas the ratios for $BR(\tau \rightarrow 3\mu)$ enter in to the allowed region by the experimental bound for large enough M_0 and/or $M_{1/2}$, the ratios for $B(\tau \rightarrow \mu\gamma)$ are well above their bound for all M_0 and $M_{1/2}$ values explored. The main point again is the particular value of θ_2 with large $|\theta_2|$ and large $\arg(\theta_2)$, which generates large rates.

With the purpose of exploring other choices of the mSUGRA parameters, we have also generated results for the specific value $A_0 = -100$ and found very close predictions to the $A_0 = 0$ case, the lines in the plots being nearly undistinguishable respect to this case. We have also run the alternative case of $\text{sign}(\mu) < 0$, and found again very close predictions to the $\text{sign}(\mu) > 0$ case, with the lines in the plots being undistinguishable from this case.

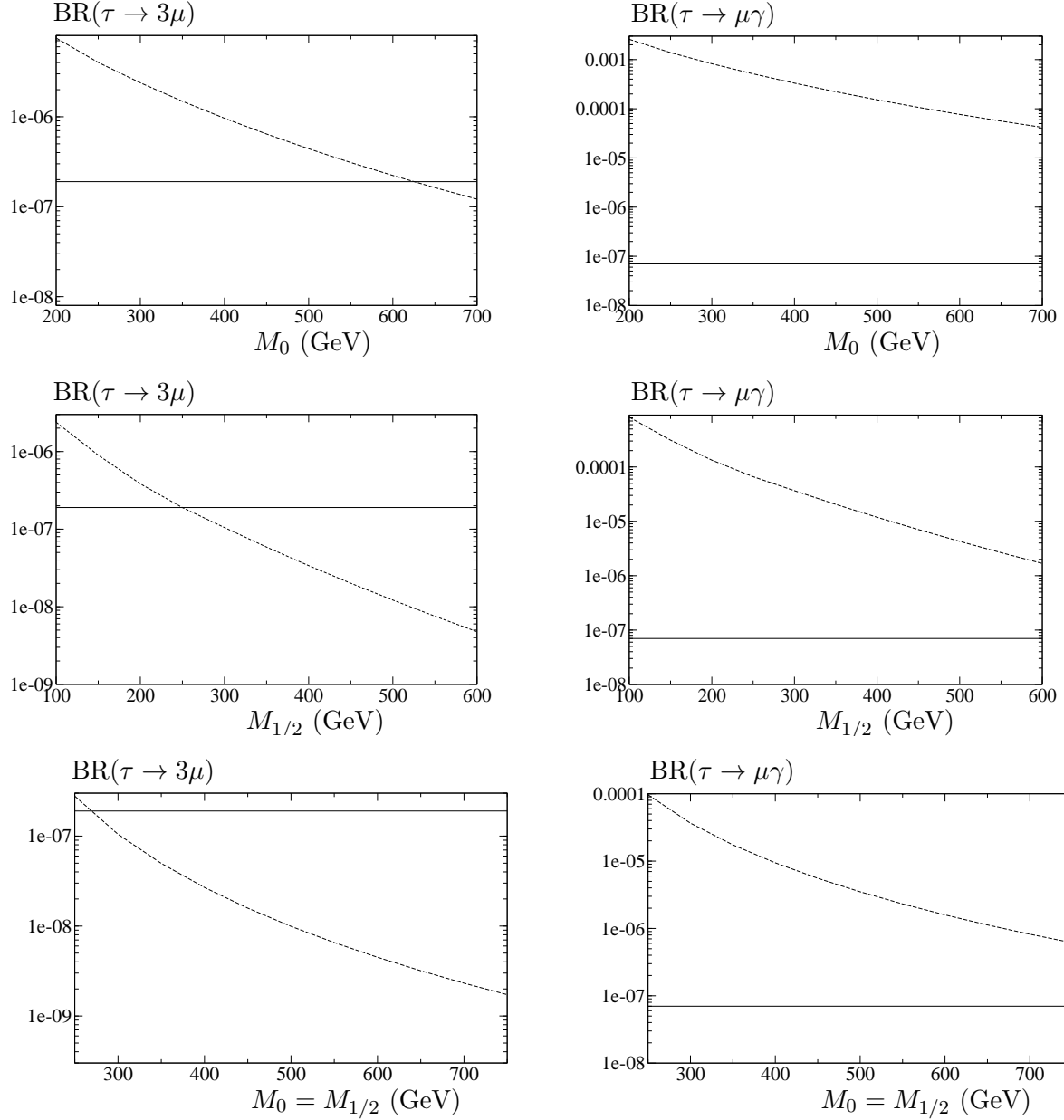


FIG. 14: Dependence of $BR(\tau^- \rightarrow \mu^- \mu^- \mu^+)$ and $BR(\tau \rightarrow \mu\gamma)$ with M_0 and $M_{1/2}$ in scenario B with hierarchical heavy neutrinos and complex R, for $(m_{N_1}, m_{N_2}, m_{N_3}) = (10^8, 2 \times 10^8, 10^{14})$ GeV, $\tan \beta = 50$, $|\theta_2| = 2.8$ and $\arg(\theta_2) = \pi/4$ ($\theta_1 = \theta_3 = 0$). (a) Upper-left panel, $BR(\tau \rightarrow \mu^- \mu^- \mu^+)$ as a function of M_0 for $M_{1/2} = 100$ GeV, (b) upper-right panel, $BR(\tau \rightarrow \mu\gamma)$ as a function of M_0 for $M_{1/2} = 100$ GeV, (c) middle-left panel, $BR(\tau \rightarrow \mu^- \mu^- \mu^+)$ as a function of $M_{1/2}$ for $M_0 = 200$ GeV, (d) middle-right panel, $BR(\tau \rightarrow \mu\gamma)$ as a function of $M_{1/2}$ for $M_0 = 200$ GeV, (e) lower-left panel, $BR(\tau \rightarrow \mu^- \mu^- \mu^+)$ as a function of $M_0 = M_{1/2}$, (f) lower-right panel, $BR(\tau \rightarrow \mu\gamma)$ as a function of $M_0 = M_{1/2}$. In all the plots we take $A_0 = 0$ and $\text{sign}(\mu) > 0$. The horizontal lines are the experimental bounds.

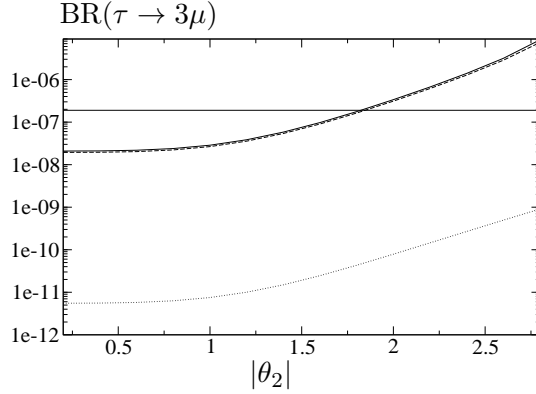


FIG. 15: Dependence of LFV $\tau \rightarrow 3\mu$ with $|\theta_2|$ in scenario B with hierarchical heavy neutrinos, for different m_{N_i} choices. Solid line is for $(m_{N_1}, m_{N_2}, m_{N_3}) = (10^8, 2 \times 10^8, 10^{14})$ GeV, dashed line is for $(m_{N_1}, m_{N_2}, m_{N_3}) = (10^{10}, 2 \times 10^{10}, 10^{14})$ GeV, and dotted line is for $(m_{N_1}, m_{N_2}, m_{N_3}) = (10^8, 2 \times 10^8, 10^{12})$ GeV. The rest of parameters are set to $\tan \beta = 50$, $M_0 = 200$ GeV, $M_{1/2} = 100$ GeV, $A_0 = 0$, $\text{sign}(\mu) > 0$ and $\arg(\theta_2) = \pi/4$. The horizontal line is the experimental bound.

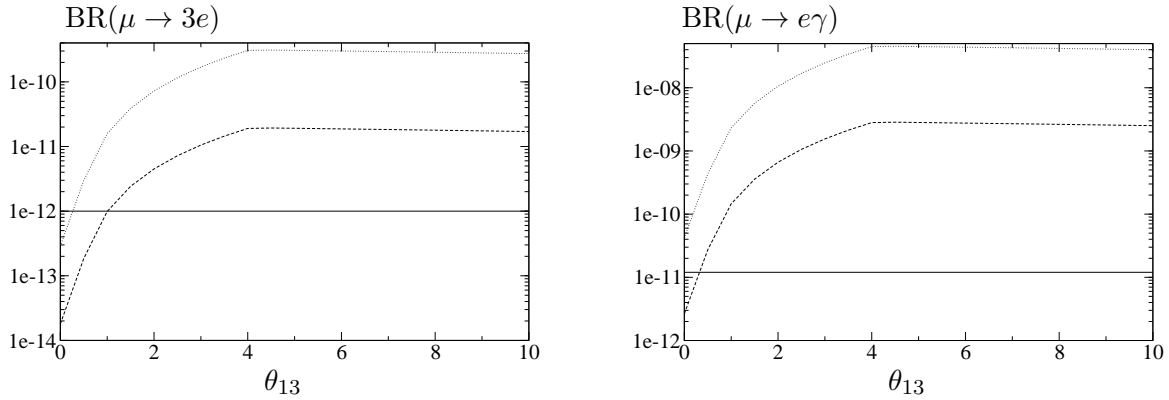


FIG. 16: Dependence of LFV μ decays with θ_{13} in degrees in scenario B with hierarchical heavy neutrinos and $R = 1$, for $(m_{N_1}, m_{N_2}, m_{N_3}) = (10^8, 2 \times 10^8, 10^{14})$ GeV, $\tan \beta = 50$, $A_0 = 0$ and $\text{sign}(\mu) > 0$. The upper lines are for $M_0 = 250$ GeV, $M_{1/2} = 150$ GeV and the lower lines are for $M_0 = 400$ GeV, $M_{1/2} = 300$ GeV. The horizontal lines are the experimental bounds.

Finally, we have also tried another input values for the heavy neutrino masses. The results for $BR(\tau \rightarrow 3\mu)$ are shown in fig. 15. Here we compare the predictions for the three following set of values, $(m_{N_1}, m_{N_2}, m_{N_3}) = (10^8, 2 \times 10^8, 10^{14})$ GeV, $(10^{10}, 2 \times 10^{10}, 10^{14})$ GeV and $(10^8, 2 \times 10^8, 10^{12})$ GeV. We conclude, that the relevant mass is the heaviest one, m_{N_3} , and the scaling with this mass is approximately as the scaling with the common mass m_N in the degenerate case. Because of this, the rates for the two first sets are nearly undistinguishable, and the rates for the third set are about four orders of magnitude below.

Last but not least, we consider the very interesting case where the angle θ_{13} of the U_{MNS} is non vanishing. It is known that the present neutrino data still allows for small values of this angle, $\theta_{13} < 10^\circ$. The dependence of $BR(\mu^- \rightarrow e^- e^- e^+)$ and $BR(\mu \rightarrow e \gamma)$ with this θ_{13} is shown in fig. 16 where we explore values in the $0 < \theta_{13} < 10^\circ$ range. We choose these two channels because they are the most sensitive ones to this angle. For this study we assume the most conservative choice of $R = 1$, and set the other parameters to the following values: $\tan \beta = 50$, $A_0 = 0$, $\text{sign}(\mu) > 0$, and $(m_{N_1}, m_{N_2}, m_{N_3}) = (10^8, 2 \times 10^8, 10^{14})$ GeV. The upper lines are for $M_0 = 250$ GeV, $M_{1/2} = 150$ GeV and the lower ones for $M_0 = 400$ GeV, $M_{1/2} = 300$ GeV. We conclude that, for this choice of parameters, values of θ_{13} larger than 1 degree are totally excluded by the data on LFV μ decays. It is a quite striking result.

In summary, we obtain in the hierachical case much larger rates than in the degenerate one, and one must pay attention to these values, because the rates in several channels do get in conflict with the experimental bounds. More specifically, the choice of a complex R matrix with large modules and/or large arguments of θ_1 and/or θ_2 and a light SUSY spectrum is very constrained by data. We also confirm that the experimental upper bounds of the processes $l_j \rightarrow l_i \gamma$ are more restrictive than the $l_j^- \rightarrow l_i^- l_i^- l_i^+$ ones but all together will allow to extract large excluded regions of the mSUGRA and seesaw parameter space. A more precise conclusion on the excluded regions of this parameter space deserves a more devoted study.

VI. CONCLUSIONS

We have shown in this paper that the LFV τ and μ decays do provide a very efficient tool to look for indirect SUSY signals. Whereas the predicted rates for these processes are negligible within the SM, the SUSY scenario considered here provides in contrast significant rates which are at the present experimental reach for some of the studied channels. This scenario consists of the well known mSUGRA extended with three right handed neutrinos and their SUSY partners, and with the needed neutrino masses being generated via the seesaw mechanism. The reason for these significant rates is because of the important lepton flavor mixing that is generated in the slepton sector due to large Yukawa neutrino couplings, which is transmited via the RGE running from the large energies down the electroweak scale.

With the motivation in mind of testing SUSY we have studied exhaustively in this work

the particular decays $\tau \rightarrow 3\mu$, $\tau \rightarrow 3e$ and $\mu \rightarrow 3e$, and the correlated radiative decays $\tau \rightarrow \mu\gamma$, $\tau \rightarrow e\gamma$ and $\mu \rightarrow e\gamma$. All of these channels have quite challenging experimental bounds and they are expected to improve in the future. We have explored the dependence of the branching ratios for these LFV processes with the various parameters involved, namely, the mSUGRA and seesaw parameters. We have computed and analyzed in full detail all the contributions from the SUSY loops to the $l_j^- \rightarrow l_i^- l_i^- l_i^+$ decays. Our analytical results for these decays correct and complete previous results in the literature. In particular we have presented the results for the separate contributions from the γ -penguin, the Z -penguin, the Higgs-penguin and the box diagrams and shown explicitly the γ -penguin dominance. In the numerical estimates we have presented results for both the $l_j^- \rightarrow l_i^- l_i^- l_i^+$ and the correlated radiative decays $l_j \rightarrow l_i\gamma$.

For the degenerate heavy neutrinos case, we have got rates for all the studied LFV τ and μ decays that are below the present experimental upper bounds. The largest rates we get, within the explored range of the seesaw and mSUGRA parameter space, are for the τ decays. Specifically, $BR(\tau \rightarrow \mu\gamma) \sim 10^{-8}$ and $BR(\tau^- \rightarrow \mu^- \mu^- \mu^+) \sim 3 \times 10^{-11}$, corresponding to the extreme values of $\tan\beta = 50$ and $m_N = 10^{14}$ GeV and for the lowest values of M_0 and $M_{1/2}$ explored. The case of hierarchical heavy neutrinos turns out to be much more interesting. First of all, we get much larger branching ratios than in the previous case and secondly they are in many cases above the present experimental bounds.

We have analyzed in detail the behaviour of the branching ratios with the mSUGRA and seesaw parameters also in the hierarchical case. The largest ratios found are again for $\tau \rightarrow \mu\gamma$ and $\tau^- \rightarrow \mu^- \mu^- \mu^+$ decays. All the LFV τ and μ decay rates are mainly sensitive to $\tan\beta$, the heaviest neutrino mass m_{N_3} , which we have set to $m_{N_3} = 10^{14}$ GeV, and the complex angles in the R matrix θ_1 and θ_2 , which have been taken in the range $3 < \tan\beta < 50$, $0 < |\theta_i| < 3$ and $0 < \arg(\theta_i) < \pi/4$. For the values of these parameters at the upper limit of this studied interval we have found that some of the predicted branching ratios are clearly above the corresponding experimental upper bounds. The most restrictive channels being $\mu \rightarrow e\gamma$, $\mu \rightarrow 3e$ and $\tau \rightarrow \mu\gamma$. Therefore, we get in this region important restrictions on the possible values of the mSUGRA and seesaw parameters. In particular, for $\theta_2 = 2.8e^{i\pi/4}$, we get that the whole studied range of $100 \text{ GeV} < M_0, M_{1/2} < 800 \text{ GeV}$ with $\tan\beta = 50$ is totally excluded by $\tau \rightarrow \mu\gamma$. Values of M_0 and $M_{1/2}$ in the low region below 250 GeV are also excluded by $\tau^- \rightarrow \mu^- \mu^- \mu^+$ data. The case of θ_1 is even more restrictive, because

the predictions for $\mu \rightarrow e\gamma$, $\mu \rightarrow 3e$ and $\tau \rightarrow \mu\gamma$ totally exclude a light SUSY scenario, for practically all θ_1 values.

Perhaps, the most striking result is that even for the most conservative choice of $R = 1$, that is $\theta_1 = \theta_2 = \theta_3 = 0$, there are also important restrictions at low M_0 , $M_{1/2}$ and large $\tan\beta$ values. In particular, for $\tan\beta = 50$, values lower or equal than $M_0 = 250$ GeV and $M_{1/2} = 150$ GeV are totally excluded by $\tau \rightarrow \mu\gamma$, $\mu \rightarrow e\gamma$ and $\mu^- \rightarrow e^-e^-e^+$ data.

For this conservative choice of $R = 1$ we have also found the surprising result that both $\mu \rightarrow e\gamma$ and $\mu^- \rightarrow e^-e^-e^+$ place important restrictions on the allowed values for the U_{MNS} angle θ_{13} . For values lower or equal than $M_0 = 250$ GeV and $M_{1/2} = 150$ GeV and for $\tan\beta = 50$ and $m_{N_3} = 10^{14}$ GeV, we get that values of θ_{13} larger than 1 degree are not allowed by these LFV data.

In conclusion, it is clear from these results that the LFV τ and μ decays studied here do restrict significantly the mSUGRA and seesaw parameter space. A more refined analysis of the restrictions on this multidimensional parameter space, deserves a further study.

Acknowledgments

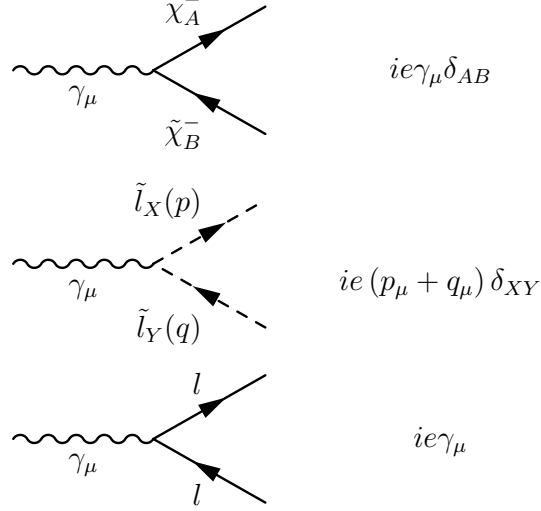
We thank the kind hospitality of the SLAC theory group members, the valuable environment for discussions there and the facilities provided at SLAC, where most of this work was done. We also thank K. Tobe for some clarifications regarding some results in [10]. M.J. Herrero acknowledges the financial support from the Spanish Ministry of Science and Education (MEC) by the grant under the name "Estancias de Profesores de Universidad en Centros Extranjeros", ref: PR2005-0069. E. Arganda acknowledges the Spanish MEC for financial support by his FPU grant AP2003-3776. This work was also supported by the Spanish MEC under project FPA2003-04597.

APPENDIX A

In this appendix we collect the Feynman rules for the interactions that are relevant in this work. They are expressed in the physical eigenstate basis, for all the MSSM sectors involved: sleptons \tilde{l}_X ($X = 1, \dots, 6$), sneutrinos $\tilde{\nu}_X$ ($X = 1, 2, 3$), neutralinos $\tilde{\chi}_A^0$ ($A = 1, \dots, 4$), charginos $\tilde{\chi}_A^\pm$ ($A = 1, 2$) and the neutral Higgs bosons H_p ($p = 1, 2, 3$) = h^0, H^0, A^0 .

1. Photon interactions

The Feynman rules for the photon interactions that are used in this work are given by,



2. Neutralino interactions

The Feynman rules for neutralinos that take part in the one-loop diagrams computed here are the following:

where

$$N_{iAX}^L = -g\sqrt{2} \left\{ \frac{m_{l_i}}{2M_W \cos \beta} N_{A3}^* R_{(1,3,5)X}^{(l)} + \tan \theta_W N_{A1}^* R_{(2,4,6)X}^{(l)} \right\} \quad (\text{A1})$$

$$N_{iAX}^R = -g\sqrt{2} \left\{ -\frac{1}{2} (\tan \theta_W N_{A1} + N_{A2}) R_{(1,3,5)X}^{(l)} + \frac{m_{l_i}}{2M_W \cos \beta} N_{A3} R_{(2,4,6)X}^{(l)} \right\} \quad (\text{A2})$$

C is the charge conjugation matrix and $P_{L,R} = \frac{1 \mp \gamma_5}{2}$. Here $R^{(l)}$ and N are the rotation matrices in the charge slepton and neutralino sectors, respectively. The definition of N can be found in [21, 22].

$$\begin{aligned}
& i (N_{iAX}^L P_L + N_{iAX}^R P_R) \\
& i (N_{iAX}^{R*} P_L + N_{iAX}^{L*} P_R) \\
& i (N_{iAX}^L P_L + N_{iAX}^R P_R) C \\
& -i C^{-1} (N_{iAX}^{R*} P_L + N_{iAX}^{L*} P_R)
\end{aligned}$$

3. Chargino interactions

The Feynman rules for the chargino interactions are given by

$$\begin{aligned}
& i (C_{iAX}^L P_L + C_{iAX}^R P_R) \\
& i (C_{iAX}^{R*} P_L + C_{iAX}^{L*} P_R)
\end{aligned}$$

where

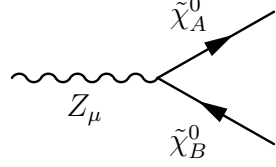
$$C_{iAX}^L = g \frac{m_{l_i}}{\sqrt{2} M_W \cos \beta} U_{A2}^* R_{(1,2,3)X}^{(\nu)} \quad (\text{A3})$$

$$C_{iAX}^R = -g V_{A1} R_{(1,2,3)X}^{(\nu)} \quad (\text{A4})$$

and $R^{(\nu)}$, U and V are the rotation matrices in the sneutrino and chargino sectors, respectively. The definitions of U and V can be found in [21, 22].

4. Z boson interactions

The Feynman rules for Z boson interactions are given by,

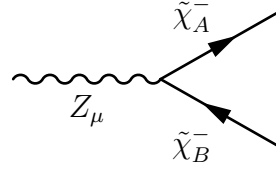


$$i\gamma_\mu \left(E_{AB}^{L(n)} P_L + E_{AB}^{R(n)} P_R \right)$$

where

$$E_{AB}^{L(n)} = \frac{g}{\cos \theta_W} O_{AB}^{\prime\prime L} = \frac{g}{c_W} \left(-\frac{1}{2} N_{A3} N_{B3}^* + \frac{1}{2} N_{A4} N_{B4}^* \right) \quad (\text{A5})$$

$$E_{AB}^{R(n)} = \frac{g}{\cos \theta_W} O_{AB}^{\prime\prime R} = -\frac{g}{c_W} \left(-\frac{1}{2} N_{A3}^* N_{B3} + \frac{1}{2} N_{A4}^* N_{B4} \right) \quad (\text{A6})$$

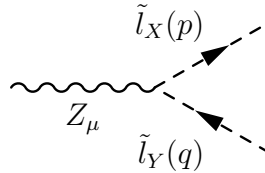


$$i\gamma_\mu \left(E_{AB}^{L(c)} P_L + E_{AB}^{R(c)} P_R \right)$$

where

$$E_{AB}^{L(c)} = -\frac{g}{\cos \theta_W} O_{AB}^{\prime R} = -\frac{g}{c_W} \left[-\left(\frac{1}{2} - s_W^2 \right) U_{A2}^* U_{B2} - c_W^2 U_{A1}^* U_{B1} \right] \quad (\text{A7})$$

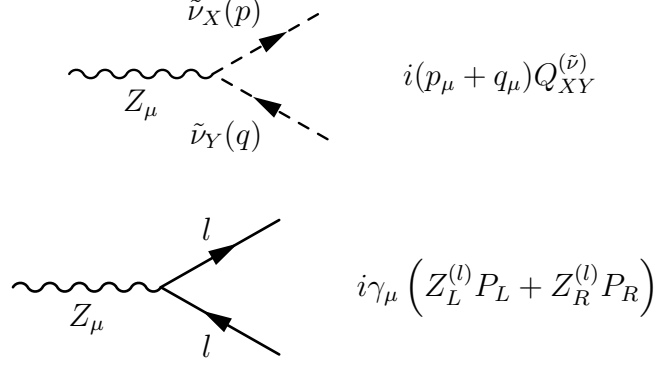
$$E_{AB}^{R(c)} = -\frac{g}{\cos \theta_W} O_{AB}^{\prime L} = -\frac{g}{c_W} \left[-\left(\frac{1}{2} - s_W^2 \right) V_{A2} V_{B2}^* - c_W^2 V_{A1} V_{B1}^* \right] \quad (\text{A8})$$



$$i(p_\mu + q_\mu) Q_{XY}^{(\tilde{l})}$$

where

$$Q_{XY}^{(\tilde{l})} = -\frac{g}{c_W} \sum_{k=1}^3 \left[\left(-\frac{1}{2} + s_W^2 \right) R_{2k-1,X}^{(l)*} R_{2k-1,Y}^{(l)} + s_W^2 R_{2k,X}^{(l)*} R_{2k,Y}^{(l)} \right] \quad (\text{A9})$$



where

$$Q_{XY}^{(\tilde{\nu})} = -\frac{g}{2c_W} \delta_{XY} \quad (\text{A10})$$

where

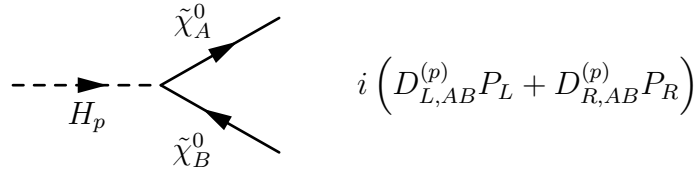
$$Z_L^{(l)} = -\frac{g}{c_W} \left[-\frac{1}{2} + s_W^2 \right] \quad (\text{A11})$$

$$Z_R^{(l)} = -\frac{g}{c_W} s_W^2 \quad (\text{A12})$$

We have used here and everywhere the short notation $s_W = \sin \theta_W$ and $c_W = \cos \theta_W$.

5. Higgs boson interactions

The Feynman rules for the three neutral Higgs bosons read as,



where

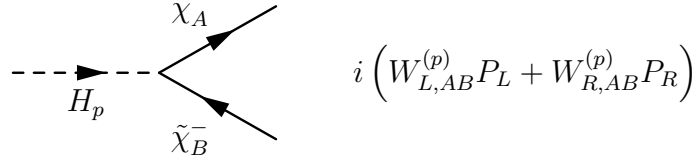
$$D_{L,AB}^{(p)} = -\frac{g}{\sin \beta} \left[Q_{BA}''^* \sigma_5^{(p)} - R_{BA}''^* \sigma_2^{(p)} + \frac{m_{\chi_A^0}}{2M_W} \sigma_2^{(p)} \delta_{BA} \right] \quad (\text{A13})$$

$$D_{R,AB}^{(p)} = -\frac{g}{\sin \beta} \left[Q_{BA}'' \sigma_5^{(p)*} - R_{BA}'' \sigma_2^{(p)*} + \frac{m_{\chi_A^0}}{2M_W} \sigma_2^{(p)*} \delta_{BA} \right] \quad (\text{A14})$$

and

$$Q_{AB}'' = \frac{1}{2} [N_{A3} (N_{B2} - \tan \theta_W N_{B1}) + N_{B3} (N_{A2} - \tan \theta_W N_{A1})] \quad (\text{A15})$$

$$R_{AB}'' = \frac{1}{2M_W} [M_2^* N_{A2} N_{B2} + M_1^* N_{A1} N_{B1} - \mu^* (N_{A3} N_{B4} + N_{A4} N_{B3})] \quad (\text{A16})$$



where

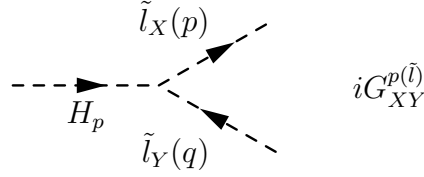
$$W_{L,AB}^{(p)} = -\frac{g}{\sin \beta} \left[Q_{BA}^* \sigma_5^{(p)} - R_{BA}^* \sigma_2^{(p)} + \frac{m_{\tilde{\chi}_A^-}}{2M_W} \sigma_2^{(p)} \delta_{BA} \right] \quad (\text{A17})$$

$$W_{R,AB}^{(p)} = -\frac{g}{\sin \beta} \left[Q_{AB} \sigma_5^{(p)*} - R_{AB} \sigma_2^{(p)*} + \frac{m_{\tilde{\chi}_A^-}}{2M_W} \sigma_2^{(p)*} \delta_{AB} \right] \quad (\text{A18})$$

and

$$Q_{AB} = \frac{1}{\sqrt{2}} U_{A2} V_{B1} \quad (\text{A19})$$

$$R_{AB} = \frac{1}{2M_W} [M_2^* U_{A1} V_{B1} + \mu^* U_{A2} V_{B2}] \quad (\text{A20})$$



where

$$\begin{aligned} G_{XY}^{p(\tilde{l})} = & -g \left[g_{LL,e}^{(p)} R_{1X}^{*(l)} R_{1Y}^{(l)} + g_{RR,e}^{(p)} R_{2X}^{*(l)} R_{2Y}^{(l)} + g_{LR,e}^{(p)} R_{1X}^{*(l)} R_{2Y}^{(l)} + g_{RL,e}^{(p)} R_{2X}^{*(l)} R_{1Y}^{(l)} \right. \\ & + g_{LL,\mu}^{(p)} R_{3X}^{*(l)} R_{3Y}^{(l)} + g_{RR,\mu}^{(p)} R_{4X}^{*(l)} R_{4Y}^{(l)} + g_{LR,\mu}^{(p)} R_{3X}^{*(l)} R_{4Y}^{(l)} + g_{RL,\mu}^{(p)} R_{4X}^{*(l)} R_{3Y}^{(l)} \\ & \left. + g_{LL,\tau}^{(p)} R_{5X}^{*(l)} R_{5Y}^{(l)} + g_{RR,\tau}^{(p)} R_{6X}^{*(l)} R_{6Y}^{(l)} + g_{LR,\tau}^{(p)} R_{5X}^{*(l)} R_{6Y}^{(l)} + g_{RL,\tau}^{(p)} R_{6X}^{*(l)} R_{5Y}^{(l)} \right] \quad (\text{A21}) \end{aligned}$$

with

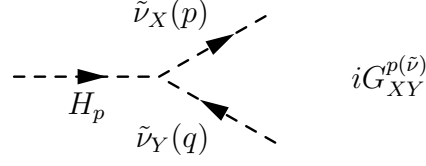
$$g_{LL,l}^{(p)} = \frac{M_Z}{\cos \theta_W} \sigma_3^{(p)} \left(\frac{1}{2} - \sin^2 \theta_W \right) + \frac{m_l^2}{M_W \cos \beta} \sigma_4^{(p)} \quad (\text{A22})$$

$$g_{RR,l}^{(p)} = \frac{M_Z}{\cos \theta_W} \sigma_3^{(p)} (\sin^2 \theta_W) + \frac{m_l^2}{M_W \cos \beta} \sigma_4^{(p)} \quad (\text{A23})$$

$$g_{LR,l}^{(p)} = \left(-\sigma_1^{(p)} A_l - \sigma_2^{(p)*} \mu \right) \frac{m_l}{2M_W \cos \beta} \quad (\text{A24})$$

$$g_{RL,l}^{(p)} = g_{LR,l}^{(p)*} \quad (\text{A25})$$

with $A_l = (A_l)^{ii} / (Y_l)^{ii}$, $i = 1, 2, 3$ for $l = e, \mu, \tau$, respectively.

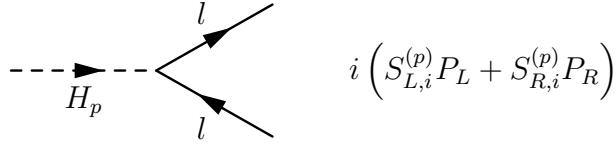


where

$$G_{XY}^{p(\tilde{\nu})} = -g \left[g_{LL,\nu}^{(p)} R_{1X}^{*(\nu)} R_{1Y}^{(\nu)} + g_{LL,\nu}^{(p)} R_{2X}^{*(\nu)} R_{2Y}^{(\nu)} + g_{LL,\nu}^{(p)} R_{3X}^{*(\nu)} R_{3Y}^{(\nu)} \right] \quad (\text{A26})$$

with

$$g_{LL,\nu}^{(p)} = -\frac{M_Z}{2 \cos \theta_W} \sigma_3^{(p)} \quad (\text{A27})$$



where

$$S_{L,i}^{(p)} = g \frac{m_{l_i}}{2M_W \cos \beta} \sigma_1^{(p)*} \quad (\text{A28})$$

$$S_{R,i}^{(p)} = S_{L,i}^{(p)*} \quad (\text{A29})$$

In all the above equations,

$$\sigma_1^{(p)} = \begin{pmatrix} \sin \alpha \\ -\cos \alpha \\ i \sin \beta \end{pmatrix} \quad (\text{A30})$$

$$\sigma_2^{(p)} = \begin{pmatrix} \cos \alpha \\ \sin \alpha \\ -i \cos \beta \end{pmatrix} \quad (\text{A31})$$

$$\sigma_3^{(p)} = \begin{pmatrix} \sin(\alpha + \beta) \\ -\cos(\alpha + \beta) \\ 0 \end{pmatrix} \quad (\text{A32})$$

$$\sigma_4^{(p)} = \begin{pmatrix} -\sin \alpha \\ \cos \alpha \\ 0 \end{pmatrix} \quad (\text{A33})$$

$$\sigma_5^{(p)} = \begin{pmatrix} -\cos(\beta - \alpha) \\ \sin(\beta - \alpha) \\ i \cos 2\beta \end{pmatrix} \quad (\text{A34})$$

and $H_p(p = 1, 2, 3) = h^0, H^0, A^0$. We have also used here the standard notation for the MSSM soft-gaugino-mass parameters $M_{1,2}$ and the μ parameter.

APPENDIX B

In this appendix we present the analytical expressions of the loop-functions for the calculations of the $l_j^- \rightarrow l_i^- l_i^- l_j^+$ decays. In these expressions we neglect the external fermion momenta/masses which for the present computation works extremely well. That is,

$$B(k^2, m_1^2, m_2^2) \simeq B(0, m_1^2, m_2^2) = B(m_1^2, m_2^2) \quad (\text{B1})$$

$$C(k_1^2, k_2^2, m_1^2, m_2^2, m_3^2) \simeq C(0, 0, m_1^2, m_2^2, m_3^2) = C(m_1^2, m_2^2, m_3^2) \quad (\text{B2})$$

$$\begin{aligned} D(k_1^2, k_2^2, k_3^2, m_1^2, m_2^2, m_3^2, m_4^2) &\simeq D(0, 0, 0, m_1^2, m_2^2, m_3^2, m_4^2) \\ &= D(m_1^2, m_2^2, m_3^2, m_4^2) \end{aligned} \quad (\text{B3})$$

1. Two-points functions

The analytical expressions for B_0 and B_1 functions are the following:

$$B_0(m_1^2, m_2^2) = -\log m_2^2 + \frac{m_2^2 - m_1^2 + m_1^2 \log\left(\frac{m_1^2}{m_2^2}\right)}{m_2^2 - m_1^2} \quad (\text{B4})$$

$$B_1(m_1^2, m_2^2) = -\frac{1}{2} + \frac{1}{2} \log m_2^2 - \frac{m_1^2 - m_2^2 + 2m_1^2 \log\left(\frac{m_2^2}{m_1^2}\right)}{4(m_1^2 - m_2^2)^2} \quad (\text{B5})$$

2. Three-points functions

The expressions for the three-points functions used in this work are given by,

$$C_0(m_1^2, m_2^2, m_3^2) = -\frac{1}{m_2^2 - m_3^2} \left(\frac{m_1^2 \log m_1^2 - m_2^2 \log m_2^2}{m_1^2 - m_2^2} - \frac{m_1^2 \log m_1^2 - m_3^2 \log m_3^2}{m_1^2 - m_3^2} \right) \quad (\text{B6})$$

$$\tilde{C}_0(m_1^2, m_2^2, m_3^2) = 1 - \frac{1}{m_2^2 - m_3^2} \left(\frac{m_1^4 \log m_1^2 - m_2^4 \log m_2^2}{m_1^2 - m_2^2} - \frac{m_1^4 \log m_1^2 - m_3^4 \log m_3^2}{m_1^2 - m_3^2} \right) \quad (\text{B7})$$

$$\begin{aligned} C_{11}(m_1^2, m_2^2, m_3^2) &= \frac{m_1^2}{2(m_1^2 - m_2^2)^2(m_1^2 - m_3^2)^2(m_2^2 - m_3^2)} \\ &\times \left[-(m_1^2 - m_2^2)(m_1^2 - m_3^2)(m_2^2 - m_3^2) + m_1^2 m_2^2 (2m_1^2 - m_2^2) \log \frac{m_1^2}{m_2^2} \right. \\ &\left. + m_1^2 m_3^2 (-2m_1^2 + m_3^2) \log \frac{m_1^2}{m_3^2} + m_2^2 m_3^2 (-2m_1^2 + m_2^2)(-2m_1^2 + m_3^2) \log \frac{m_2^2}{m_3^2} \right] \end{aligned} \quad (\text{B8})$$

$$\begin{aligned} C_{12}(m_1^2, m_2^2, m_3^2) &= \frac{1}{2(m_1^2 - m_2^2)(m_1^2 - m_3^2)^2(m_2^2 - m_3^2)^2} \\ &\times \left[(m_1^2 - m_2^2)(m_1^2 - m_3^2)(m_2^2 - m_3^2)m_3^2 + m_2^4 m_3^2 (2m_1^2 - m_3^2) \log \frac{m_2^2}{m_3^2} \right. \\ &\left. + m_1^4 \left(m_2^2 \log \frac{m_1^2}{m_2^2} + m_3^2 (-2m_2^2 + m_3^2) \log \frac{m_1^2}{m_3^2} \right) \right] \end{aligned} \quad (\text{B9})$$

$$C_{24}(m_1^2, m_2^2, m_3^2) = \frac{1}{4} \tilde{C}_0(0, 0, m_1^2, m_2^2, m_3^2) \quad (\text{B10})$$

3. Four-points functions

Finally, the four-points functions have the following expressions,

$$\begin{aligned}
 D_0(m_1^2, m_2^2, m_3^2, m_4^2) = & -\frac{m_1^2 \log m_1^2}{(m_1^2 - m_2^2)(m_1^2 - m_3^2)(m_1^2 - m_4^2)} + \frac{m_2^2 \log m_2^2}{(m_1^2 - m_2^2)(m_2^2 - m_3^2)(m_2^2 - m_4^2)} \\
 & -\frac{m_3^2 \log m_3^2}{(m_1^2 - m_3^2)(m_2^2 - m_3^2)(m_3^2 - m_4^2)} + \frac{m_4^2 \log m_4^2}{(m_1^2 - m_4^2)(m_2^2 - m_4^2)(m_3^2 - m_4^2)}
 \end{aligned} \tag{B11}$$

$$\begin{aligned}
 \tilde{D}_0(m_1^2, m_2^2, m_3^2, m_4^2) = & -\frac{m_1^4 \log m_1^2}{(m_1^2 - m_2^2)(m_1^2 - m_3^2)(m_1^2 - m_4^2)} + \frac{m_2^4 \log m_2^2}{(m_1^2 - m_2^2)(m_2^2 - m_3^2)(m_2^2 - m_4^2)} \\
 & -\frac{m_3^4 \log m_3^2}{(m_1^2 - m_3^2)(m_2^2 - m_3^2)(m_3^2 - m_4^2)} + \frac{m_4^4 \log m_4^2}{(m_1^2 - m_4^2)(m_2^2 - m_4^2)(m_3^2 - m_4^2)}
 \end{aligned} \tag{B12}$$

-
- [1] B. T. Cleveland *et al.*, *Astrophys. J.* **496** (1998) 505; W. Hampel *et al.*, *Phys. Lett. B* **447** (1999) 127; Q. R. Ahmad *et al.* [SNO Collaboration], *Phys. Rev. Lett.* **87** (2001) 071301 [arXiv:nucl-ex/0106015]; Q. R. Ahmad *et al.* [SNO Collaboration], *Phys. Rev. Lett.* **89** (2002) 011302 [arXiv:nucl-ex/0204009]. R. Becker-Szendy *et al.*, *Nucl. Phys. Proc. Suppl.* **38**, 331 (1995). Y. Fukuda *et al.* [Kamiokande Collaboration], *Phys. Lett. B* **335**, 237 (1994); Y. Ashie *et al.* [Super-Kamiokande Collaboration], *Phys. Rev. Lett.* **93**, 101801 (2004) [arXiv:hep-ex/0404034]. T. Araki *et al.* [KamLAND Collaboration], *Phys. Rev. Lett.* **94**, 081801 (2005) [arXiv:hep-ex/0406035]; E. Aliu *et al.* [K2K Collaboration], *Phys. Rev. Lett.* **94**, 081802 (2005) [arXiv:hep-ex/0411038]; T. Araki *et al.* [KamLAND Collaboration], *Phys. Rev. Lett.* **94**, 081801 (2005) [arXiv:hep-ex/0406035].
- [2] Z. Maki, M. Nakagawa and S. Sakata, *Prog. Theor. Phys.* **28** (1962) 870; B. Pontecorvo, *Zh. Eksp. Teor. Fiz.* **33** (1957) 549 and **34** (1957) 247.
- [3] M. Gell-Mann, P. Ramond, and R. Slansky, *Complex spinors and unified theories*, in *Supergravity* (P. van Nieuwenhuizen and D. Z. Freedman, eds.), North Holland, Amsterdam, 1979, p. 315; Pierre Ramond, CALT-68-709, Feb 1979. 21pp. Invited talk given at Sanibel Symposium, Palm Coast, Fla., Feb 25 - Mar 2, 1979; hep-ph/9809459; T. Yanagida, in *Proceedings of the Workshop on the Unified Theory and the Baryon Number in the Universe* (O. Sawada and A. Sugamoto, eds.), KEK, Tsukuba, Japan, 1979, p. 95; S. L. Glashow, *The future of*

- elementary particle physics*, in *Proceedings of the 1979 Cargèse Summer Institute on Quarks and Leptons* (M. Lévy, J.-L. Basdevant, D. Speiser, J. Weyers, R. Gastmans, and M. Jacob, eds.), Plenum Press, New York, 1980, pp. 687–713; R. N. Mohapatra and G. Senjanović, *Phys. Rev. Lett.* **44**, 912 (1980).
- [4] F. Borzumati and A. Masiero, *Phys. Rev. Lett.* **57**, 961 (1986).
- [5] B. Aubert *et al.* [BABAR Collaboration], *Phys. Rev. Lett.* **92**, 121801 (2004) [arXiv:hep-ex/0312027].
- [6] U. Bellgardt *et al.* [SINDRUM Collaboration], *Nucl. Phys. B* **299**, 1 (1988).
- [7] B. Aubert *et al.* [BABAR Collaboration], *Phys. Rev. Lett.* **95**, 041802 (2005) [arXiv:hep-ex/0502032].
- [8] B. Aubert *et al.* [BABAR Collaboration], arXiv:hep-ex/0508012.
- [9] M. L. Brooks *et al.* [MEGA Collaboration], *Phys. Rev. Lett.* **83** (1999) 1521 [arXiv:hep-ex/9905013].
- [10] J. Hisano, T. Moroi, K. Tobe and M. Yamaguchi, *Phys. Rev. D* **53** (1996) 2442 [arXiv:hep-ph/9510309].
- [11] J. Hisano, D. Nomura and T. Yanagida, *Phys. Lett. B* **437**, 351 (1998) [arXiv:hep-ph/9711348]; J. Hisano and D. Nomura, *Phys. Rev. D* **59**, 116005 (1999) [arXiv:hep-ph/9810479]; W. Buchmuller, D. Delepine and F. Vissani, *Phys. Lett. B* **459**, 171 (1999) [arXiv:hep-ph/9904219]; J. R. Ellis, M. E. Gomez, G. K. Leontaris, S. Lola and D. V. Nanopoulos, *Eur. Phys. J. C* **14**, 319 (2000) [arXiv:hep-ph/9911459]; X. J. Bi, Y. B. Dai and X. Y. Qi, *Phys. Rev. D* **63**, 096008 (2001) [arXiv:hep-ph/0010270]; J. Hisano and K. Tobe, *Phys. Lett. B* **510**, 197 (2001) [arXiv:hep-ph/0102315]; X. J. Bi and Y. B. Dai, *Phys. Rev. D* **66**, 076006 (2002) [arXiv:hep-ph/0112077]; D. F. Carvalho, J. R. Ellis, M. E. Gomez, S. Lola and J. C. Romao, *Phys. Lett. B* **618**, 162 (2005) [arXiv:hep-ph/0206148]; S. Lavignac, I. Masina and C. A. Savoy, *Phys. Lett. B* **520**, 269 (2001) [arXiv:hep-ph/0106245]; Y. Kuno and Y. Okada, *Rev. Mod. Phys.* **73**, 151 (2001) [arXiv:hep-ph/9909265]; J. R. Ellis, J. Hisano, M. Raidal and Y. Shimizu, *Phys. Rev. D* **66**, 115013 (2002) [arXiv:hep-ph/0206110]; F. Deppisch, H. Pas, A. Redelbach, R. Ruckl and Y. Shimizu, *Eur. Phys. J. C* **28**, 365 (2003) [arXiv:hep-ph/0206122]; A. Dedes, J. R. Ellis and M. Raidal, *Phys. Lett. B* **549**, 159 (2002) [arXiv:hep-ph/0209207]; J. Hisano, arXiv:hep-ph/0209005; S. Pascoli, S. T. Petcov and C. E. Yaguna, *Phys. Lett. B* **564**, 241 (2003) [arXiv:hep-ph/0301095]; T. Fukuyama, T. Kikuchi and N. Okada, *Phys. Rev. D* **68**,

- 033012 (2003) [arXiv:hep-ph/0304190]; J. I. Illana and M. Masip, Eur. Phys. J. C **35**, 365 (2004) [arXiv:hep-ph/0307393]; A. Masiero, S. K. Vempati and O. Vives, New J. Phys. **6**, 202 (2004) [arXiv:hep-ph/0407325].
- [12] J. A. Casas and A. Ibarra, Nucl. Phys. B **618** (2001) 171 [arXiv:hep-ph/0103065].
- [13] K. S. Babu and C. Kolda, Phys. Rev. Lett. **89**, 241802 (2002) [arXiv:hep-ph/0206310].
- [14] J. R. Ellis, J. Hisano, M. Raidal and Y. Shimizu, Phys. Rev. D **66**, 115013 (2002) [arXiv:hep-ph/0206110].
- [15] A. Brignole, A. Rossi, Phys. Lett. **B566**, 217 (2003), hep-ph/0304081.
- [16] E. Arganda, A. M. Curiel, M. J. Herrero and D. Temes, Phys. Rev. D **71**, 035011 (2005) [arXiv:hep-ph/0407302].
- [17] A. Brignole and A. Rossi, Nucl. Phys. B **701**, 3 (2004) [arXiv:hep-ph/0404211].
- [18] P. Paradisi, arXiv:hep-ph/0508054.
- [19] J. K. Parry, arXiv:hep-ph/0510305.
- [20] S. Eidelman *et al.* [Particle Data Group], Phys. Lett. B **592**, 1 (2004).
- [21] H. E. Haber and G. L. Kane, *The search for supersymmetry: probing physics beyond the standard model*, Phys. Rept. **117**, 75 (1985).
- [22] J. F. Gunion and H. E. Haber, *Higgs bosons in supersymmetric models. 1*, Nucl. Phys. **B272**, 1 (1986). [E: **B402**, 569 (1993)]
- [23] Y. Grossman and H. E. Haber, Phys. Rev. Lett. **78** (1997) 3438 [arXiv:hep-ph/9702421].
- [24] P. H. Chankowski, J. R. Ellis, S. Pokorski, M. Raidal and K. Turzyski, Nucl. Phys. B **690** (2004) 279 [arXiv:hep-ph/0403180].
- [25] X. J. Bi, B. Feng and X. m. Zhang, arXiv:hep-ph/0309195.
- [26] M. C. Gonzalez-Garcia and C. Pena-Garay, Phys. Rev. D **68** (2003) 093003 [arXiv:hep-ph/0306001].
- [27] W. Porod, Comput. Phys. Commun. **153**, 275 (2003) [arXiv:hep-ph/0301101].
- [28] F. Gabbiani, E. Gabrielli, A. Masiero, L. Silvestrini, Nucl. Phys. **B477**, 321 (1996).
- [29] P. H. Chankowski, O. Lebedev and S. Pokorski, arXiv:hep-ph/0502076.
- [30] P. Paradisi, arXiv:hep-ph/0505046.
- [31] W. Hollik, in *Precision Tests of the Standard Electroweak Model*, edited by P. Langacker (World Scientific, Singapore, 1995), pp. 37–116;